DMD Fast Forward. Published on March 10, 2017 as DOI: 10.1124/dmd.116.073940
This article has not been copyedited and formatted. The final version may differ from this version.

DMD # 73940

Metabolite Identification, Reaction Phenotyping and Retrospective Drug-Drug Interaction Predictions of 17-deacetylnorgestimate, the Active Component of the Oral Contraceptive Norgestimate

Deepak Ahire, Sarmistha Sinha, Barry Brock, Ramaswamy Iyer, Sandhya Mandlekar and Murali Subramanian

Pharmaceutical Candidate Optimization, Biocon Bristol-Myers Squibb R&D Center (BBRC), Syngene International Ltd, Plot No. 2 & 3, Bommasandra IV Phase, Jigani Link Road, Bangalore-560100: D.A., S.S., M.S

Pharmaceutical Candidate Optimization, Bristol-Myers Squibb, 311Pennington Rocky Hill Road, Pennington, NJ 08534: B.B., R.I.

Pharmaceutical Candidate Optimization, Bristol-Myers Squibb India Ltd. BBRC, Bangalore, India: S.M.

DMD Fast Forward. Published on March 10, 2017 as DOI: 10.1124/dmd.116.073940
This article has not been copyedited and formatted. The final version may differ from this version.

Running title: Predicting 17-deacetylnorgestimate Drug-Drug Interactions

Author contact information

Murali Subramanian, murali.subramanian@syngeneintl.com

Biocon Bristol-Myers Squibb Research and Development Center (BBRC), Syngene International Limited, Biocon Park Plot 2 & 3 Bommasandra IV Phase Bangalore - 560 099, India

Phone number: 91-80-66334061

Number of text pages: 26

Number of tables: 4

Number of Figures: 9

Number of references: 46

Number of words in abstract: 246

Number of words in introduction: 732

Number of words in discussion: 1532

Number of figures in supplement: 4

Abbreviations:

17-deacetylnorgestimate (NGMN); area under the plasma concentration vs time curve (AUC); atazanavir (ATV); maximal plasma concentration (C_{max}); recombinant CYPs (rCYPs); cytochrome P450s (CYPs); drug-drug interactions (DDIs), ethinyl estradiol (EE); efavirenz (EFZ); fraction of a drug metabolized by a particular enzyme (f_m);human liver microsomes (HLM); ketoconazole (KTZ); lopinavir (LPR); liquid chromatography-mass spectrometry (LC-MS); nicotinamide adenine dinucleotide phosphate (NADPH); norgestrel (NG); orthotricyclen (OTC); protease inhibitors (PI); ritonavir (RTV); tris (hydroxymethyl)-aminomethane hydrochloride (Tris-HCl); uridine 5′-diphosphoglucuronic acid (UDPGA); uridine 5'-diphospho-glucuronosyltransferases (UGTs); recombinant UGTs (rUGTs)

DMD Fast Forward. Published on March 10, 2017 as DOI: 10.1124/dmd.116.073940
This article has not been copyedited and formatted. The final version may differ from this version.

Abstract

Ortho-Tri-Cyclen® (OTC), a two drug cocktail comprising of ethinylestradiol (EE) and norgestimate (13-ethyl-17-acetoxy-18, 19-dinor-17α-pregn-4-en-20yn-3 oxime), is commonly prescribed to avert unwanted pregnancies in women of reproductive age. *In vivo*, norgestimate undergoes extensive and rapid deacetylation to produce 17-deacetylnorgestimate (NGMN), an active circulating metabolite that likely contributes significantly to norgestimate efficacy. Despite being of primary significance, the metabolism and reaction phenotyping of NGMN have not been previously reported. Hence, detailed biotransformation and reaction phenotyping studies of NGMN with recombinant cytochrome P450s (rCYPs), recombinant uridine 5'-diphospho-glucuronosyltransferases (rUGTs) and human liver microsomes (HLM) in the presence and absence of selective cytochrome P450 (CYP) inhibitors were conducted. It was found that cytochrome P450 3A4 (CYP3A4) plays a key role in NGNM metabolism with a fraction metabolized (f_m) of 0.57. CYP2B6 and to an even lesser extent CYP2C9 were also observed to catalyze NGMN metabolism. Using this CYP3A4 f_m, the predicted area under the plasma concentration vs. time curve (AUC) change in NGMN using a basic/mechanistic static model was found to be within 1.3-fold of reported NGMN AUC changes for four modulators of CYP3A4. In addition to NGMN, we have also elucidated the biotransformation of norgestrel (NG), a downstream norgestimate and NGMN metabolite, and found that CYP3A4 and UGT1A1 have a major contribution to the elimination of NG with a combined f_m of 1. The data presented in this manuscript will lead to a better understanding and management of NGMN based drug-drug interactions (DDIs) when norgestimate is co-administered with CYP3A4 modulators.

DMD Fast Forward. Published on March 10, 2017 as DOI: 10.1124/dmd.116.073940
This article has not been copyedited and formatted. The final version may differ from this version.

Introduction

Orthotricyclen® (OTC) is commonly prescribed to avert unwanted pregnancies in women of reproductive age, and is increasingly recommended as hormone replacement therapy to manage menopausal symptoms. It consists of 0.035 mg of ethinylestradiol (EE), and 0.18 or 0.215 or 0.25 mg of norgestimate (Schwartz et al., 2009). It contains 2 hormones- aprogestin (norgestimate), which suppresses ovulation and an estrogen (EE) which suppresses production of follicle-stimulating hormone and luteinizing hormone (Becker, 1990; Corson, 1990; McGuire et al., 1990; Huber, 1991; Bringer, 1992; Kafrissen, 1992; Kaplan, 1995). Since OTC is prescribed to prevent pregnancy, maintaining efficacious levels of its components is crucial. However, this is complicated by the fact that the active components of OTC are very susceptible to drug-drug interactions (DDIs), with numerous DDIs reported thus far (Weblink 2015). These DDIs have usually been attributed to modulation of cytochrome P450 3A4 (CYP3A4) activity (Hariparsad et al., 2004; Zhang et al., 2011).

Norgestimate (13-ethyl-17-acetoxy-18, 19-dinor-17α-pregn-4-en-20yn-3 oxime; norgestrel-3-oxime-17-acetate) is a synthetic steroid which possesses anti-progestational and anti-fertility activity (Becker, 1990; Corson, 1990; McGuire et al., 1990; Huber, 1991; Bringer, 1992; Kafrissen, 1992; Kaplan, 1995). Current understanding suggests that norgestimate is a prodrug and 17-deacetylnorgestimate (NGMN) is the active metabolite that likely exerts efficacy. Norgestimate and NGMN likely have equivalent potencies but NGMN has much higher systemic exposures, and hence likely contributes to contraceptive action much more than norgestimate (McGuire et al., 1990; Kafrissen, 1992). In the preclinical species of rats, dogs and monkey, orally administered ^{14}C norgestimate was rapidly absorbed with maximum radioactivity being detected in plasma within 4h of administration and with an elimination half life of 30 to

DMD Fast Forward. Published on March 10, 2017 as DOI: 10.1124/dmd.116.073940
This article has not been copyedited and formatted. The final version may differ from this version.

67h. In women, ^{14}C norgestimate was also rapidly absored with maximal circulating radioactivity observed in 30 min to 2h and eliminated with a terminal half life of 45 to 71h (Alton et al., 1984; McGuire et al., 1990; Kaplan, 1995; Schwartz et al., 2009). Upon oral administration of 0.18 mg of norgestimate, the peak norgestimate serum concentrations were only 270 pM whereas NGMN concentrations were greater than 12 nM 1h after dosing, and high concentrations were seen even 36h after dosing (Alton et al., 1984; McGuire et al., 1990; Kaplan, 1995; Schwartz et al., 2009). Hence, the long circulating radioactivity half-life likely stems from NGMN and not norgestimate.

In vitro, it was found that norgestimate is rapidly decaetylated in multiple matrices to produce NGMN which is subsequently metabolized to produce norgestrel (NG) that undergoes further metabolism (Madden and Back, 1991; Wild et al., 1991; Wild et al., 1993). In human liver microsome (HLM) preps, NGMN was formed in the absence of nicotinamide adenine dinucleotide phosphate (NADPH) from norgestimate, whereas in the presence of NADPH, NGMN, 3-keto norgestimate, NG and other metabolites were formed. Normal colon samples, human endometrial cancer cell lines (HEC-1A), endometrial tissue, stomach tissue, normal and malignant breast cells in culture were also found to convert norgestimate to NGMN (Madden and Back, 1991; Wild et al., 1993). As such, cytochrome P450 (CYP) expression is not expected in these cells, suggesting that a wide variety of hydrolytic enzymes are capable of converting norgestimate to NGMN. The fact that norgestimate metabolism is fundamentally catalyzed by enzymes other than CYPs, and in multiple tissues and organs, makes norgestimate resistant to DDIs, since such DDIs are typically mediated through CYPs. In contrast, NGMN metabolism was found to be NADPH dependent, and a significant correlation was observed between NGMN metabolism and CYP content (Madden and Back, 1991). To summarize, norgestimate is

DMD Fast Forward. Published on March 10, 2017 as DOI: 10.1124/dmd.116.073940
This article has not been copyedited and formatted. The final version may differ from this version.

metabolized rapidly to an active metabolite, NGMN, which circulates at efficacious concentrations with a long elimination half-life and likely contributes significantly to efficacy. Currently, there is no understanding of the enzyme families responsible for the clearance of NGMN and NG. Hence, to predict and enable a retrospective understanding of NGMN and NG DDIs, metabolite identification and reaction phenotyping studies were undertaken to determine CYP and uridine 5'-diphospho-glucuronosyltransferases (UGT) isoforms involved in NGMN and NG metabolism. NGMN DDIs have been reported when lopinavir (LPR)/ritonavir (RTV) or RTV/atazanavir (ATV) or efavirenz (EFZ) were co-administered with norgestimate; the actual fold-AUC changes were compared with retrospectively calculated predicted AUC changes based on the determined fraction metabolized (f_m) value of CYP3A4 (Vogler et al., 2010; Sevinsky et al., 2011; Zhang et al., 2011). Our data and analyses from these studies and would lead to more effective management of clinical trials and marketed drug use in women of child bearing potential who have been prescribed norgestimate.

Materials and Methods:

Chemicals: Norgestimate ($C_{23}H_{31}NO_3$), norethindrone ($C_{20}H_{26}O_2$), napthoflavone ($C_{19}H_{12}O_2$), thio TEPA($C_6H_{12}N_3PS$) , quercetin ($C_{15}H_{10}O_7$), sulphaphenazole ($C_{15}H_{14}N_4O_2S$), benzylnirvanol ($C_{18}H_{18}N_2O_2$), quinidine ($C_{20}H_{24}N_2O$), GSH ($C_{10}H_{17}N_3O_6S$), CYP3cide ($C_{26}H_{32}N_8$), ketoconazole (KTZ, $C_{26}H_{28}Cl_2N_4O_4$), ATV ($C_{38}H_{52}N_6O_7$), NGMN ($C_{21}H_{29}NO_2$) and NG ($C_{21}H_{28}O_2$) were purchased from Sigma Aldrich (St. Louis, USA). HPLC grade acetonitrile (ACN, C_2H_3N), methanol (CH_4O), formic acid (H_2CO_2), potassium dihydrogen phosphate (KH_2PO_4) and dipotassium hydrogen phosphate (K_2HPO_4) were purchased from Merck Specialties Private Limited (Mumbai, India). NADPH ($C_{21}H_{29}N_7O_{17}P_3$) was purchased from (Sisco research laboratory Ltd. Mumbai) and five mixed gender pooled HLM, recombinant uridine 5'-diphospho-glucuronosyltransferases (rUGTs) and recombinant cytochrome P450s (rCYPs) were purchased from Corning (New York, USA).

Instruments: Liquid chromatography mass spectrometry (LC-MS) systems used in the study were as follows: (1) LC-MS Orbitrap™ (Thermo Scientific, Bremen, Germany) equipped with Agilent (Santa Clara, CA) 1200 HPLC for *in vitro* incubations in HLM, (2) QTRAP® 5500 (AB Sciex, Concord, Ontario, Canada) equipped with Waters (Milford, MA) ACQUITY® UPLC for reaction phenotyping.

***In vitro* Incubations in HLM for Metabolite Profiling of NGMN and NG.**

A typical CYP microsomal assay was carried out in HLM with NGMN and NG, wherein both NGMN and NG (30μM) were separately pre-incubated with HLM (1mg/mL) in phosphate buffer

(0.1 M)at pH 7.4 for 5 min. Reactions were initiated by addition of NADPH (1mM) and incubated for 60 min at 37^{o}C in a total reaction volume of 1000µL. Control incubations were performed in the absence of NADPH. At 0 and 60 min, 300 µL aliquots were taken and quenched with an equal volume of acetonitrile to precipitate the proteins. Then the reaction mixture was vortexed, centrifuged at 14000 × g for 10 min and the resulting supernatants analyzed in the LTQ-Velos Orbitrap.

For determination of NADPH and UGT-mediated metabolism, both NGMN and NG (30µM) were pre-incubated in Tris-HCl buffer (0.1 M) at a pH of 7.4 containing 10mM $MgCl_2$ and 1mg/mL alamethacin treated HLM. The HLM was pretreated for 20 min with alamethacin (50µg/mg protein) on ice. The reaction was initiated by the addition of uridine 5′-diphosphoglucuronic acid (UDPGA, 3mM) and NADPH (1mM). The incubations and sample processing were carried out in a similar fashion as described above, and samples were analyzed by LTQ-Velos Orbitrap. Control experiments were performed in the absence of NADPH and UDPGA.

Reaction Phenotyping:

In a typical assay, both NGMN and NG (1µM) were pre-incubated for 5 min with rCYPs 3A4, 3A5, 2C9, 2C8, 2C19, 2D6, 1A2, 2E1, 2A6, 2B6 (25 nM) in 96 well plates containing phosphate buffer (0.1 M) at pH 7.4. The reaction was initiated by addition of NADPH (1mM) and incubated for 60 min at 37^{o}C. Aliquots were taken 0, 3, 15 and 60 min, and quenched with two volumes of acetonitrile containing norethindrone as an internal standard. Sample processing was carried out in a similar fashion as described in the previous section and analyzed by UPLC-

MS/MS. Reaction phenotyping of NGMN was also performed with HLM in the presence of specific inhibitors. The selective CYP inhibitors were alpha-napthoflavone (CYP1A1 inhibitor at 1μM), thio-TEPA (CYP2B6, 50μM), quercetin (CYP2C8, 20μM), sulphaphenazole (CYP2C9, 10μM), benzylnirvanol (CYP2C19, 1μM), quinidine (CYP2D6, 1μM), CYP3cide (CYP3A4, 1μM) and KTZ (CYP3A4 and CYP3A5, 1μM). Thio-TEPA and CYP3cide are mechanism based inhibitors; hence, both those inhibitors were pre-incubated with HLM and NAPDH mixture for 15 min and reaction was initiated by addition of NGMN (1μM). For other inhibitors, a mixture of NGMN (1 μM), HLM (1 mg/ml) and inhibitors were pre-incubated for 5 min and reaction was initiated by addition of NADPH (1mM). The reaction was incubated for 60 min at 37^{o}C and aliquots were taken at 0, 30 and 60 min and quenched with two volumes of acetonitrile containing norethindrone as an internal standard, samples were processed for analysis as described previously. To determine UGT activity, NGMN and NG (1μM) were pre-incubated with rUGTs 1A1, 1A4, 1A6, 2B4, 2B7 (1mg/mL) in 96 well plates, with alamethacin pretreatment, as described in the previous section. The reaction was initiated by addition of UDPGA (5mM) followed by an incubation of 45 min at 37^{o}C. Aliquots were taken at 0, 5, 15, 30 and 45 min. Additionally in a separate incubation, NG (1μM) was incubated with rUGT1A1 (1mg/mL) and UDPGA (5mM) for 5 min with aliquots taken at 0, 1, 2, 3, 4 and 5 min. Samples were processed and analyzed as previously described in this section. In another set of incubations, NG (1μM) was incubated with alamethacin treated HLM (1mg/ml) as previously described, with and without KTZ (CYP3A4 and CYP3A5 inhibitor at 1μM) and ATV (UGT1A1 and CYP3A4/3A5 inhibitor at 1μM). The reaction was initiated by addition of NADPH (1mM) and UDPGA (5mM). The incubation was carried out at 37^{o}C for 45 min and aliquots were taken at 0, 5, 15, 30 and 45 min and samples were processed as previously described.

DMD Fast Forward. Published on March 10, 2017 as DOI: 10.1124/dmd.116.073940
This article has not been copyedited and formatted. The final version may differ from this version.

Determination of f_m:

f_m values for NGMN was determined from their incubation in the presence and absence of specific inhibitors in HLM, whereas f_m values for NG was determined from separate incubations of NG with and without KTZ and ATV, as described in the previous section. The initial rate of disappearance (k_{el}) of NGMN and NG in the presence and absence of inhibitors was determined by plotting the natural log of % disappearance versus time; fm was calculated using Equations 1, as described in Yang et al (Yang et al., 2016). Sufficient turnover to calculate an elimination rate constant and $t_{1/2}$ value was assessed by determining if the elimination slope was statistically different from zero.

Equation 1

$$\% \, Inhibition = 100 * \frac{k_{el,no\ inh} - k_{el,with\ inh}}{k_{el,no\ inh}}$$

$$f_m = \frac{\% \, Inhibition}{Sum\ of\ Total\ \% \, Inhibition\ across\ CYP\ isoforms}$$

Prediction of NGMN DDIs:

Based on a survey of literature, significant NGMN (as a victim) DDIs were observed in three studies where LPR/RTV, RTV/ATV or EFZ were co-administered with norgestimate (Vogler et al., 2010; Sevinsky et al., 2011; Zhang et al., 2011). Other studies also reported victim DDIs of NGMN but had insufficient data to facilitate retrospective calculations. The University of Washington Drug-Drug Interaction database was queried for induction, reversible and

irreversible inhibition of LPR, RTV, ATV and EFZ and the values are summarized in Table 1. NGMN victim DDIs were predicted using the equation (Equation 2) from the FDA guidance document with the incorporation of f_m of CYP3A4 determined from our studies (U.S. Department of Health and Human Services, 2012).

Equation 2:

$$\frac{AUC_I}{AUC} = \frac{1}{(A_h \times B_h \times C_h) \times f_m + (1 - f_m)}$$

wherein AUC_i/AUC is the predicted ratio of NGMN area under of the plasma concentration versus time curve (AUC) in the presence and absence of the inhibitor; f_m the fraction metabolized of NGMN by the affected CYP. Only the hepatic component of inhibition has been considered since Fg (intestinal availability) data, a key parameter governing the extent of inhibition, for the inhibitors is not available

A_h, B_h and C_h are the terms for reversible inhibition, irreversible inhibition and induction of the perpetrators, respectively, and are defined in Equations 3, 4 and 5.

Equation 3

$$A = \frac{1}{1 + \frac{[I]_h}{K_i}}$$

Where $[I]_h$ is the *in vivo* inhibitor concentration of the perpetrator and K_i is the perpetrator reversible inhibitor constant.

.

Equation 4

$$B = \frac{1}{1 + \frac{[I]_h \times k_{inact}}{k_{deg} \times (K_I + [I]_h)}}$$

where K_I the perpetrator irreversible inactivator inhibition constant, k_{inact} the maximum inactivation rate constant of the perpetrator and k_{deg} the *in vivo* first order degradation rate constant of the affected CYP,

Equation 5

$$C = 1 + \frac{d \times E_{max} \times [I]_h}{[I]_h + EC_{50}}$$

where E_{max} is the fold induction in enzyme activities of the perpetrator, EC_{50} the perpetrator concentration of inducer causing half maximal induction. d was assumed to be 1 as advised in the FDA guidance (U.S. Department of Health and Human Services, 2012).

Three values of $[I]_h$ were used in the equation: total maximal plasma concentration (C_{max}), unbound C_{max}(f_u*C_{max}) and the unbound portal vein concentration from Equation 6 (U.S. Department of Health and Human Services, 2012).

Equation 6:

$$[\boldsymbol{I}]_{\boldsymbol{h}} = \boldsymbol{f_u} \times [\boldsymbol{I}]_{\boldsymbol{max}} + \frac{\boldsymbol{F_a} \times \boldsymbol{K_a} \times \boldsymbol{Dose}}{\boldsymbol{Q_h}}$$

DMD Fast Forward. Published on March 10, 2017 as DOI: 10.1124/dmd.116.073940
This article has not been copyedited and formatted. The final version may differ from this version.

where f_u is the fraction of the inhibitor unbound in blood of the perpetrator, I_{max} is C_{max} of the perpetrator, F_a the fraction absorbed after oral administration of the perpetrator , K_a the first order absorption rate constant of the perpetrator and Q_h the hepatic blood flow.

For the purposes of these calculations, the following values were assumed.

k_{deg}: 0.000321 min^{-1}; Fa: 1; Ka: 0.1 min^{-1}; Qh: 1.5 L/min. These are the conservative values for DDI predictions as mentioned in the FDA guidance (U.S. Department of Health and Human Services, 2012). f_u for LPR, RTV, ATV and EFZ were obtained from literature as 0.008, 0.0027, 0.135 and 0.006 (Almond et al., 2005; Zhang et al., 2005; Kalvass et al., 2007; Aweeka et al., 2010; Delille et al., 2014).

Results.

Metabolite Profile of NGMN in HLM

A typical LC/MS chromatogram of NGMN metabolites produced in NADPH and UDPGA supplemented HLM is shown in Figure 1. NGMN, eluted at 28.31 min. In addition to NGMN, seven metabolites including NG (denoted as Met 7) and other oxidative metabolites (denoted as Met 1, Met 2, Met 3, Met 4, Met 5 and Met 6) were detected. These metabolites eluted at 15.77 min (Met 1), 16.55 min (Met 2), 19.49 min (Met 3), 21.35 min (Met 4), 24.14 min (Met 5), 26.47min (Met 6) and 27.02min (Met 7) (Figure 1 and Supplement Figure 2). The relative abundance of parent and metabolites is shown in Table 2; the predominant metabolic pathway was CYP mediated oxidation and hydrolysis of oxime moiety into ketone to produce NG. Trace amounts of a glucuronide were detected by MS only.

The structures of metabolites of NGMN were elucidated based on exact mass and product ion mass spectral analysis (Supplement Figure 2).NGMN displayed molecular ion peak of 328.2271. The product ion spectra of NGMN exhibited characteristic daughter ion peaks at m/z 310.2165, 292.206, 260.2009, 264.1747, 124.0754 and 282.1852 (Figure 2). The product ions of m/z 310.2165 and 292.2060 were produced by water loss. The ion of m/z 260.2009 is a result of C-C bond cleavage and simultaneous removal of but-3-yn-2-ol from cyclopentane ring. The ions of m/z 264.1747 and 282.1852 were produced by removal of the ethyl moiety and by water loss. The ion 124.0754 resulted from cleavage of C-C bond and removal of methyloctahydro-1H-inden-1-ol which corresponded to 5-hydroxyimino cyclohex-3-enyl methylium ion. Oxidative metabolites denoted as Met1 and Met 3-6 exhibited a molecular ion peak at m/z 344.222, an addition of 15.9949 Da to the molecular ion of NGMN at m/z 328.2271 suggesting mono-hydroxylation of parent. The presence of fragment ion of m/z 124.0754 as unaltered and addition

of 15.9949 Da to the fragment ions of m/z 310.2165, 264.1747 and 124.0754 in Met1 suggested that oxidation took place on decahydronaphthalene ring. The molecular ion peak of Met2 was 360.2169; an addition of 31.9898 Da to the molecular ion of NGMN at m/z 328.2271 suggesting di-hydroxylation of parent. The CID spectra of Met2 exhibited ions at m/z 342.2064, 324.1958, 280.1696, 124.0757 and 298.1802 suggesting addition of 31.9898 Da to fragment ions of m/z 310.2165 and 292.2060, addition of 15.9949 Da to the fragments of m/z 264.1747 and 282.1852; however fragment of m/z 124.0754 remained which implied that di-hydroxylation had occurred on both decahydrophenanthren ring and ethyl moiety.The product ion spectra of Met3 exhibited modification of m/z 310.216, 292.2060 and 260.2009 fragment ions by addition of 15.9949 Da; however fragment of m/z 124.0754 was remained unaltered suggesting hydroxylation had occurred on ethyldecahydronaphthalene ring. The collision-induced dissociation spectra of Met 4 revealed addition of 15.9949 Da to the fragment ions of m/z 310.2465, 292.2060 and 260.2009 whereas fragments of m/z 124.0754 and 282.1852 remained unaltered which indicated that oxidation had occurred on ethyl moiety. The presence of unaltered fragmentations of m/z 260.2009,124.0754 and the addition of 15.9949 Da to the fragment ion of m/z 292.2060 in Met5 suggested that oxidation had occurred on cyclopentane ring. The product ion spectra of Met6 exhibited ions at m/z 326.2115, 308.2009, 276.1958 and 280.1696 suggesting addition of 15.9949 Da to the fragment ions of m/z 310.2165, 292.2060, 260.2009 and 264.1747 which indicated oxidation had occurred on decahydrophenanthren ring.

Metabolite Profile of NG in HLM

In HLM supplemented by NADPH and UDPGA six hydroxylated metabolites (denoted as Met 8, Met 10-14) and one glucuronide metabolite of NG (assigned as Met 9) were detected as the most

abundant metabolites by both UV and MS (Figure 3). The retention time of NG and its metabolites were 27.04 min (NG), 17.94 min (Met 8), 18.63 min (Met 9), 20.49 min (Met 10), 20.74 min (Met 11), 21.16 min (Met 12), 22.06 min (Met 13) and 22.36 min (Met 14). The relative abundance of parent and metabolites are shown in Table 3. The predominant metabolic pathways of NG were found to be NADPH dependent oxidation and glucuronidation. The structures of metabolites of NG were elucidated based on exact mass and product ion mass spectral analysis (Supplement figure 3). NG displayed molecular ion peak of 313.2163. The product ion spectra of NG exhibited characteristic daughter ion peaks at m/z 295.205, 277.1951, 267.1743, 245.19, 237.1638 and 109.0648 (Figure 4). The product ions of m/z 295.2050 and 277.1951 were produced by water loss. The daughter ions of m/z 267.1743and 245.1900 were produced by removal of ethyl moiety, simultaneous water loss from the cyclopentane ring and by cleavage of a C-C bond and simultaneous removal of but-3-yn-2-ol from the cyclopentane ring, respectively. The product ion of m/z 237.1638 was formed by removal of prop-2-yn-1-ol from the cyclopentane ring and further water loss. The daughter ion of m/z 109.0648 was produced from cleavage of a C-C bond and removal of methyloctahydro-1H-inden-1-ol which corresponded to 5-oxocyclohex-3-enyl methylene ion. Oxidative metabolites denoted as Met 8 and Met 10-14 exhibited a molecular ion peak of m/z 329.2111, an addition of 15.9949 Da to the molecular ion of NG at m/z 313.2162 suggesting mono-hydroxylation of parent. The collision ion dissociation spectra of Met 8, Met 10 and Met 12 exhibited ions of m/z 293.19 and 243.1743 suggesting the addition of 15.9949 Da followed by water loss to the fragment ions of m/z 295.2050 and 245.1900 while fragment ion of m/z 109.0648 remained unaltered which implies that oxidation occurred on the ethyldecahydronaphthalene ring in the case of Met8, M10 and M12. The CID spectra of Met11 revealed addition of 15.9949 Da to the fragment ions of m/z

295.2050, 277.1951 and addition of 15.9949 Da followed by water loss to fragment ion of m/z 245.1900 whereas fragment ions of m/z 267.1743 and 109.0648 remained unaltered which indicated that oxidation had occurred on the ethyl moiety. The presence of fragment ions of m/z 245.1900 and 109.0648 as unaltered and addition of 15.9949 Da to the fragment ion of m/z 295.2050 and 277.1951 in Met 14 suggested that oxidation had occurred in the cyclopentane ring. The product ion spectra of Met 13 exhibited addition of 15.9949 Da to the fragment ions of m/z 295.2050 and 277.1951G and addition of 15.9949 Da followed by water loss to fragment ion of m/z 245.1900 suggesting oxidation had occurred on the decahydrophenanthren ring containing ethyl moiety. The product ion spectra of Met 9 exhibited intense daughter ion peak at m/z 313.2162, corresponding to NG, which was produced by 176 neutral loss which ischaracteristic of glucuronide conjugation of the –OH attached to the cyclopentane ring. The putative metabolic pathway of NGMN and NG is shown in Figure 5.

Metabolism of NGMN in the Presence of rCYPs and HLM.

Initial screening of NGMN with rCYP isoforms exhibited rapid metabolism of NGMN in presence of rCYP3A4 whereas no significant turnover of parent was observed in case of other rCYPs (Figure 6, Supplement Figure 1). Metabolite formation of NGMN was also analyzed in rCYPs (Figure 7) and CYP2C9 and CYP2B6 show the formation of Met 1, Met 3 and Met 4. CYP3A5 did not form significant amount of any metabolite. Hence CYP3A4 was the predominant isoform involved in the metabolism of NGMN with minor contributions from CYP2B6 and CYP2C9. Interestingly, Met 3 which was formed by CYP2B6 and CYP2C9 at 3 min were further metabolized at 30 min illustrating the importance of early time point measurements.

DMD Fast Forward. Published on March 10, 2017 as DOI: 10.1124/dmd.116.073940
This article has not been copyedited and formatted. The final version may differ from this version.

In HLM, selective inhibitors KTZ (CYP3A4 and CYP3A5), CYP3cide (CYP3A4) and thio-TEPA (CYP2B6) substantially inhibited the disappearance of NGMN (Figure 8, panel A). Both KTZ and CYP3cide almost completely inhibited the disappearance of NGMN, suggesting that CYP3A4 played a predominant role in NGMN metabolism, consistent with results from the rCYPs. Thio-TEPA also inhibited the metabolism of NGMN by around 50%. Metabolite formation of NGMN also revealed the same trend (Figure 8, panel B-F). At 30 min, Met 1,3,4,5 and 6 formations were inhibited in the presence of thio-TEPA whereas Met 1, 3 and 4 were inhibited in the presence of sulphaphenazole (CYP2C9 inhibitor). Formation of all metabolites was inhibited by greater than 90% by KTZ and CYP3cide, consistent with parent disappearance data. Hence, based on the HLM data, CYP3A4 plays a major role in NGMN disappearance with minor contributions from CYP2B6 and CYP2C9. The f_m for CYP3A4 and CYP2B6 was determined as per Equation 1, using the HLM in the presence of inhibitors data, and were found to be 0.57 and 0.43 respectively.

Metabolism of NG in the Presence of rCYPs and HLM.

Turnover of NG was observed only in presence of rCYP3A4 and rUGT1A1 whereas no turnover was observed in case of other rCYPs and rUGTs (Supplement Figure 1, 4). In HLM, NG depletion was inhibited by 60% and 100% in the presence of KTZ and ATV. This translated to an f_m of 0.6 for CYP3A4 and a combined f_m of 1 for CYP3A4 plus UGT1A1. In the presence of KTZ, M2 to M7 formation was inhibited by more than 90%, whereas Met 1 formation was inhibited by 60%

DDI Prediction

DMD Fast Forward. Published on March 10, 2017 as DOI: 10.1124/dmd.116.073940
This article has not been copyedited and formatted. The final version may differ from this version.

Predicted fold-AUC changes for NGMN (as a victim) upon co-administration of LPR, RTV, ATV and EFZ (perpetrators) were determined using the equations described previously, and the *in vitro* values shown in Table 4. For both ATV/RTV and LPR/RTV co-administered perpetrators, the fold NGMN AUC increase predicted was between 2.1 to 2.3 fold while the observed fold change in NGMN AUC increase was around 1.8-fold. Hence, the predicted and actual DDI predictions were very close to each other. Irrespective of which inhibitor concentration was used- total C_{max}, free C_{max} or the portal vein concentration, the predicted fold AUC changes of NGMN was between 2.1 and 2.3 fold. When total perpetrator C_{max} and portal vein concentrations of the inhibitor were used, the NGMN AUC fold change was ~2.3-fold. For EFZ, the predicted fold decrease in NGMN AUC was 0.35 (65% reduction in AUC) when total C_{max} was used and 0.70 when the portal vein concentration was used. When free C_{max} was included in the equation only a 10% reduction in AUC was predicted. The observed AUC fold-reduction was 0.36 (64% reduction in AUC) very similar to the 0.35 fold change predicted using total C_{max}. All predicted and observed AUC changes are summarized in Table 4.

DMD Fast Forward. Published on March 10, 2017 as DOI: 10.1124/dmd.116.073940
This article has not been copyedited and formatted. The final version may differ from this version.

Discussion

Maintaining efficacious levels of the active OTC components in women of child bearing age avoiding pregnancy is very important. While EE (a component of OTC) metabolism is well studied and DDIs can be rationalized, norgestimate is more complex. Norgestimate by itself does not circulate but forms an active metabolite NGMN, and determining the altered exposures of NGMN is important. Until now, the metabolism and disposition of norgestimate had been studied in numerous studies, but the metabolism of NGMN was not investigated.

The metabolites of NGMN (Figure 5) are hydroxylation on decahydronaphthalene ring (Met 1), di-hydroxylation on ethyl, dodecahydro-1H-cyclopentanaphthalene moiety to produce (Met 2), hydroxylation on ethyl decahydronaphthalene (Met 3), hydroxylation on ethyl moiety to produce (Met 4), hydroxylation on cyclopentane ring to form (Met 5), hydroxylation on decahydrophenanthren 2(3-H) oxime (Met 6) and deoximation to produce NG (Met 7). The metabolic pathway of NG (Figure 5) includes oxidation on ethyl and cyclopentane moiety to produce Met 11 and Met 14 respectively, oxidation on ethyldecahydronaphthalene (Met 8, Met 10 and Met 12) hydroxylation on dodecahydrophenanthrene ring (Met 13) and direct glucuronidation on OH group to produce Met 9.

The reaction phenotyping results clearly indicate a dominant role for CYP3A4-mediated metabolism of NGMN (f_m of 0.57) with a lesser role for CYP2B6, even lesser role for CYP2C9 and no role for CYP3A5. The implication of CYP3A4 in the metabolism of NGMN is consistent with numerous clinical trial wherein it was found that daclatasvir, alitretinoin, rosuvastatin, rifaximin, laropiprant, sofosbuvir, ledipasvir, dolutegravir, dexloxiglumide, tenofovir disoproxil fumarate (a prodrug of tenofovir), saxaglipitin and raltegravir did not influence the exposures of

NGMN (Simonson et al., 2004; Roy et al., 2005; Kearney and Mathias, 2009; Schwartz et al., 2009; Anderson et al., 2011; Schmitt-Hoffmann et al., 2011; Upreti et al., 2012; Bifano et al., 2014; German et al., 2014; Song et al., 2015). The lack of an interaction is consistent with the data presented in this manuscript, since none of these compounds are inducers/inhibitors of CYP3A4. In contrast, compounds that inhibit or induce CYP3A4 such as cobicistat, LPR/RTV combination, RTV/ATV combination and EFZ significantly altered the exposure and PK of NGMN (Vogler et al., 2010; Polina German, 2011; Sevinsky et al., 2011; Zhang et al., 2011). A fixed dose combination ofelvitegravir/cobicistat/emtricitabine/tenofovir disoproxil fumarate increased NGMN's exposure by greater than 2-fold which is consistent with cobicistat's irreversible CYP3A4 inhibition properties (Polina German, 2011). 300 mg/100 mg of ATV/RTV caused a 68, 85 and 102% increase in C_{max}, AUC, C_{24h} for NGMN (Zhang et al., 2011). In another study, patch NGMN AUC increased by 83% when LPR/RTV (400/100mg) were co-administered with the OTC (Vogler et al., 2010). In light of our data showing that NGMN is a substrate of CYP3A4, the increases in C_{max} are reasonable since LPR, RTV and ATV are CYP3A4 inhibitors. A 46, 62 and 84% decrease in NGMN C_{max}, AUC and C_{24h} were observed when 600 mg (daily dosing) of EFZ was co-administered with OTC (14 days of co-dosing) (Sevinsky et al., 2011). No effect was observed on EE PK parameters. EFZ is an inducer of CYP3A4 *in vivo*, which could explain the reason for NGMN exposures declining substantially (Siccardi et al., 2013). EFZ also decreased NG exposures by 60-80% consistent with the fact that NG is metabolized by CYP3A4 and UGT1A1 (Sevinsky et al., 2011). It should be mentioned that in the ATV/RTV and LPR/RTV DDI studies, there was a reduction in EE exposure which was offset by increases in NGMN exposure. Hence, in both these studies the authors did not anticipate a loss in contraceptive efficacy despite the observed DDIs. In contrast, when EFZ was

co-administered, there was no effect on EE AUC but significantly reduced NGMN levels which prompted the authors to recommend barrier contraception to overcome loss of efficacy.

DDI predictions are summarized in Table 4 and show that in all inhibition DDI instances, the observed and predicted DDI were within 1.3 fold of each other. In the case of LPR/RTV and ATV/RTV co-administration, when either free, total perpetrator C_{max} or free portal vein concentrations was utilized there was very minimal impact on the NGMN AUC prediction even though the inhibitor concentrations were several fold apart. Since the perpetrators are potent irreversible and reversible inhibitors, even the free C_{max} is high enough to cause maximal inhibition. Hence, the only factor governing NGMN DDI is f_m, and the maximal DDI change is essentially $1/(1-f_m)$ which is 2.3-fold which, in turn, is very close to the observed 1.8-fold change. If the perpetrators are also CYP2B6 and CYP2C9 inhibitors, a higher AUC change can be expected. In the case of induction by EFZ, when total C_{max} concentration was considered the predicted AUC change was around 0.36 (64% decline in NGMN AUC), almost identical to the observed change of 0.35. The predicted to actual AUC changes were larger when free C_{max} and portal vein concentrations were used (1.9 to 2.5 fold difference). Therefore, in the case of inhibition and induction, the actual NGMN AUC changes are very close to the observed NGMN AUC changes when total C_{max} values of the perpetrator are considered.

In order to determine which parameter had the greatest impact on predicted fold NGMN AUC changes, a sensitivity analysis was performed wherein the values of fm, K_I, k_{inact} and inhibitor concentration were varied over a wide range (Figure 9). From these analyses, it is clear that NGMN f_m has the most dramatic effect on fold NGMN AUC change. The AUC change was from 1 to greater than 300-fold as f_m ranged from 0 to 1 (Figure 9A). In contrast, C_{max} had a minimal effect on fold AUC (Figure 9B). At very low perpetrator C_{max} values (close to 1 nM),

DMD Fast Forward. Published on March 10, 2017 as DOI: 10.1124/dmd.116.073940
This article has not been copyedited and formatted. The final version may differ from this version.

the fold AUC change was ~1. From a C_{max} of 100 nM onwards the fold AUC changed reached 2-fold and did not vary much thereafter plateauing at a 2.3-fold AUC change. Another important observation is that even though a combination of inhibitors was used (LPR/RTV or ATV/RTV), the fold AUC change was not additive consistent with the fact that C_{max} had a minimal impact on AUC change in the sensitivity analyses. Perpetrator k_{inact} and KI values also did not have a dramatic impact on fold AUC change (Figure 9C and 9D).

DDIs involving PIs are usually complex and paradoxical since they not only inhibit CYP3A4 but also induce CYP3A4 and CYP2B6. For example, at steady state, RTV does not change oral clearance of alprazolam but a single dose of RTV reduces the oral clearance of alprazolam (Liu et al., 2012). Additionally, upon chronic administration, RTV is capable of auto-induction despite CYP3A4 reversible and irreversible inhibition (Kirby et al., 2011). The EC_{50} and E_{max} for RTV induction of 3A4 have been incorporated into our DDI predictions but for LPR and ATV such data is not available. Additionally, while all three PIs have the potential to induce CYP3A4 and CYP2B6 at the transcript level, this induction may be masked by reversible and irreversible inhibition at the activity level and hence accurate E_{max} and EC_{50} values are unavailable (Kharasch et al., 2008; Kirby et al., 2011; Liu et al., 2012). In our studies we predicted a 2.3-fold increase in AUC based on the fm of 0.57 but the observed AUC changes were around 1.8-fold. Induction of CYP3A4 and CYP2B6 could boost metabolism compensating for the inhibition leading to the lower AUC changes than predicted.

An accurate measure of F_g is essential to assess DDIs due to intestinal inhibition but such data is not available in the literature for the compounds under scrutiny. For low F_g compounds, a lot of the drug is in the intestine to exert its inhibitory and the extent of inhibition is high, and vice-versa for compounds with a high F_g. ATV and RTV have a high oral bioavailabilities (>60%)

signifying a high F_g (Zeldin and Petruschke, 2004; Colombo et al., 2006; Rathbun and Liedtke, 2011). Additionally, combination PIs have even greater %F than individually dosed PIs due to an inhibition of metabolism as evidenced by the multi-fold increase in AUC values. Given the high F_g values likely for all PIs the AUC change due to intestinal inhibition is likely to be low. Since accurate Fg values were not available, and the impact of intestinal inhibition was likely to be low, we have not included it in our analyses.

Norgestimate is a widely prescribed contraceptive agent and owes its efficacy to its active metabolite NGMN, whose levels are likely to be altered when enzymes involved in its metabolism are inhibited or induced. Any perturbations of NGMN levels will likely lead to adverse events or loss of efficacy. Hence, understanding and predicting NGMN DDIs is very important to safe implementation of a norgestimate dosing regimen. The data presented in this manuscript enables a prospective understanding of NGMN DDIs.

In summary, detailed biotransformation studies of both NGMN and NG in HLM demonstrated that NGMN was metabolized to produce NG and several oxidative metabolites whereas NG undergoes biotransformation to produce several oxidative metabolites and a glucuronide metabolite. The CYP3A4 f_m values of NGMN was determined as 0.57 and the NGMN AUC changes observed in several clinical DDI studies were found to be within 1.3 fold of the predicted AUC changes.

Authorship Contributions

Participated in research design: Ahire, Sinha, Brock, Iyer, Mandlekar and Subramanian

Conducted experiments: Ahire, Sinha

Contributed new reagents or analytic tools: not applicable

Performed data analysis: Ahire, Sinha, and Subramanian

Wrote or contributed to the writing of the manuscript: Ahire, Sinha, Iyer, Mandlekar and Subramanian

References:

(2015). "Interactions between Antiretrovirals (ARVs) and Hormonal Contraceptives ". Retrieved October, 2016, from http://hivclinic.ca/main/drugs_interact_files/Oral%20Contraceptive-int.pdf.

Almond LM, Hoggard PG, Edirisinghe D, Khoo SH, and Back DJ (2005) Intracellular and plasma pharmacokinetics of efavirenz in HIV-infected individuals. *Journal of antimicrobial Chemotherapy* **56**: 738-744.

Alton KB, Hetyei NS, Shaw C, and Patrick JE (1984) Biotransformation of norgestimate in women. *Contraception* **29**: 19-29.

Anderson MS, Hanley WD, Moreau AR, Jin B, Bieberdorf FA, Kost JT, Wenning LA, Stone JA, Wagner JA, and Iwamoto M (2011) Effect of raltegravir on estradiol and norgestimate plasma pharmacokinetics following oral contraceptive administration in healthy women. *Br J Clin Pharmacol* **71**: 616-620.

Aweeka FT, Stek A, Best BM, Hu C, Holland D, Hermes A, Burchett SK, Read J, Mirochnick M, Capparelli EV, and the International Maternal Pediatric Adolescent ACTGPPT (2010) Lopinavir protein binding in HIV-1-infected pregnant women. *HIV Medicine* **11**: 232-238.

Becker H (1990) Supportive European data on a new oral contraceptive containing norgestimate. *Acta Obstet Gynecol Scand Suppl* **152**: 33-39.

Bifano M, Sevinsky H, Hwang C, Kandoussi H, Jiang H, Grasela D, and Bertz R (2014) Effect of the coadministration of daclatasvir on the pharmacokinetics of a combined oral contraceptive containing ethinyl estradiol and norgestimate. *Antivir Ther* **19**: 511-519.

Bringer J (1992) Norgestimate: a clinical overview of a new progestin. *Am J Obstet Gynecol* **166**: 1969-1977.

Colombo S, Buclin T, Franc C, Guignard N, Khonkarly M, Tarr PE, Rochat B, Biollaz J, Telenti A, and Decosterd LA (2006) Ritonavir-boosted atazanavir-lopinavir combination: a pharmacokinetic interaction study of total, unbound plasma and cellular exposures. *Antivir Ther* **11**: 53.

Corson SL (1990) Efficacy and clinical profile of a new oral contraceptive containing norgestimate. U.S. clinical trials. *Acta Obstet Gynecol Scand Suppl* **152**: 25-31.

Delille CA, Pruett ST, Marconi VC, Lennox JL, Armstrong WS, Arrendale RF, Sheth AN, Easley KA, Acosta EP, and Vunnava A (2014) Effect of protein binding on unbound atazanavir and darunavir cerebrospinal fluid concentrations. *The Journal of Clinical Pharmacology* **54**: 1063-1071.

Ernest CS, 2nd, Hall SD, and Jones DR (2005) Mechanism-based inactivation of CYP3A by HIV protease inhibitors. *J Pharmacol Exp Ther* **312**: 583-591.

Fahmi OA, Maurer TS, Kish M, Cardenas E, Boldt S, and Nettleton D (2008) A combined model for predicting CYP3A4 clinical net drug-drug interaction based on CYP3A4 inhibition, inactivation, and induction determined in vitro. *Drug Metabolism and Disposition* **36**: 1698-1708.

German P, Moorehead L, Pang P, Vimal M, and Mathias A (2014) Lack of a clinically important pharmacokinetic interaction between sofosbuvir or ledipasvir and hormonal oral contraceptives norgestimate/ethinyl estradiol in HCV-uninfected female subjects. *J Clin Pharmacol* **54**: 1290-1298.

Hariparsad N, Nallani SC, Sane RS, Buckley DJ, Buckley AR, and Desai PB (2004) Induction of CYP3A4 by efavirenz in primary human hepatocytes: comparison with rifampin and phenobarbital. *J Clin Pharmacol* **44**: 1273-1281.

Huber J (1991) Clinical experience with a new norgestimate-containing oral contraceptive. *Int J Fertil* **36 Suppl 1**: 25-31.

Hyland R, Dickins M, Collins C, Jones H, and Jones B (2008) Maraviroc: in vitro assessment of drug-drug interaction potential. *Br J Clin Pharmacol* **66**: 498-507.

Kafrissen ME (1992) A norgestimate-containing oral contraceptive: review of clinical studies. *Am J Obstet Gynecol* **167**: 1196-1202.

Kalvass JC, Maurer TS, and Pollack GM (2007) Use of Plasma and Brain Unbound Fractions to Assess the Extent of Brain Distribution of 34 Drugs: Comparison of Unbound Concentration Ratios to in Vivo P-Glycoprotein Efflux Ratios. *Drug Metabolism and Disposition* **35**: 660-666.

Kaplan B (1995) Desogestrel, norgestimate, and gestodene: the newer progestins. *Ann Pharmacother* **29**: 736-742.

Kearney BP, and Mathias A (2009) Lack of effect of tenofovir disoproxil fumarate on pharmacokinetics of hormonal contraceptives. *Pharmacotherapy* **29**: 924-929.

Kharasch ED, Mitchell D, Coles R, and Blanco R (2008) Rapid Clinical Induction of Hepatic Cytochrome P4502B6 Activity by Ritonavir. *Antimicrob Agents Chemother* **52**: 1663-1669.

Kirby BJ, Collier AC, Kharasch ED, Dixit V, Desai P, Whittington D, Thummel KE, and Unadkat JD (2011) Complex Drug Interactions of HIV Protease Inhibitors 2: In Vivo Induction and In Vitro to In Vivo Correlation of Induction of Cytochrome P450 1A2, 2B6 and 2C9 by Ritonavir or Nelfinavir. *Drug Metabolism and Disposition* **39** 2329-2337.

Liu L, Mugundu GM, Kirby BJ, Samineni D, Desai PB, and Unadkat JD (2012) Quantification of human hepatocyte cytochrome P450 enzymes and transporters induced by HIV protease inhibitors using newly validated LC-MS/MS cocktail assays and RT-PCR. *Biopharmaceutics & Drug Disposition* **33**: 207-217.

Madden S, and Back DJ (1991) Metabolism of norgestimate by human gastrointestinal mucosa and liver microsomes in vitro. *J Steroid Biochem Mol Biol* **38**: 497-503.

McGuire JL, Phillips A, Hahn DW, Tolman EL, Flor S, and Kafrissen ME (1990) Pharmacologic and pharmacokinetic characteristics of norgestimate and its metabolites. *Am J Obstet Gynecol* **163**: 2127-2131.

Polina German MW, David Warren, Brian Kearney (2011). Pharmacokinetic Interaction Between Norgestima/Ethinyl Estradiol and EVG/COBI/FTC/TDF Single Tablet Regimen. 12th International Workshop on Clinical Pharmacology of HIV Therapy. Miami, Florida.

Rathbun RC, and Liedtke MD (2011) Antiretroviral drug interactions: overview of interactions involving new and investigational agents and the role of therapeutic drug monitoring for management. *Pharmaceutics* **3**: 745-781.

Roy P, Jakate AS, Patel A, Abramowitz W, Wangsa J, Persiani S, and Kapil R (2005) Effect of multiple-dose dexloxiglumide on the pharmacokinetics of oral contraceptives in healthy women. *J Clin Pharmacol* **45**: 329-336.

Schmitt-Hoffmann AH, Roos B, Sauer J, Schleimer M, Schoetzau A, Leese PT, Weidekamm E, and Maares J (2011) Influence of alitretinoin on the pharmacokinetics of the oral contraceptive ethinyl estradiol/norgestimate. *Clin Exp Dermatol* **36 Suppl 2**: 4-11.

Schwartz JI, Liu F, Wang YH, Pramanik B, Johnson-Levonas AO, Gutierrez MJ, Lai E, and Wagner JA (2009) Effect of laropiprant, a PGD2 receptor 1 antagonist, on estradiol and norgestimate pharmacokinetics after oral contraceptive administration in women. *Am J Ther* **16**: 487-495.

Sevinsky H, Eley T, Persson A, Garner D, Yones C, Nettles R, Krantz K, Bertz R, and Zhang J (2011) The effect of efavirenz on the pharmacokinetics of an oral contraceptive containing ethinyl estradiol and norgestimate in healthy HIV-negative women. *Antivir Ther* **16**: 149-156.

Siccardi M, Olagunju A, Seden K, Ebrahimjee F, Rannard S, Back D, and Owen A (2013) Use of a physiologically-based pharmacokinetic model to simulate artemether dose adjustment for overcoming the drug-drug interaction with efavirenz. *In Silico Pharmacol* **1**: 4.

Simonson SG, Martin PD, Warwick MJ, Mitchell PD, and Schneck DW (2004) The effect of rosuvastatin on oestrogen & progestin pharmacokinetics in healthy women taking an oral contraceptive. *Br J Clin Pharmacol* **57**: 279-286.

Song IH, Borland J, Chen S, Wajima T, Peppercorn AF, and Piscitelli SC (2015) Dolutegravir Has No Effect on the Pharmacokinetics of Oral Contraceptives With Norgestimate and Ethinyl Estradiol. *Ann Pharmacother* **49**: 784-789.

U.S. Department of Health and Human Services FDA (2012) Drug Interaction Studies —Study Design, Data Analysis, Implications for Dosing, and Labeling Recommendations.

Upreti VV, Hsiang CB, Li L, Xu X, LaCreta FP, and Boulton DW (2012) Effect of saxagliptin on the pharmacokinetics of the active components of Ortho-Cyclen((R)), a combined oral contraceptive containing ethinyl estradiol and norgestimate, in healthy women. *Diabetes Obes Metab* **14**: 1155-1157.

Vogler MA, Patterson K, Kamemoto L, Park JG, Watts H, Aweeka F, Klingman KL, and Cohn SE (2010) Contraceptive efficacy of oral and transdermal hormones when co-administered with protease inhibitors in HIV-1-infected women: pharmacokinetic results of ACTG trial A5188. *J Acquir Immune Defic Syndr* **55**: 473-482.

Weemhoff JL, Moltke LL, Richert C, Hesse LM, Harmatz JS, and Greenblatt DJ (2003) Apparent mechanism-based inhibition of human CYP3A in-vitro by lopinavir. *Journal of pharmacy and pharmacology* **55**: 381-386.

Wild MJ, Rudland PS, and Back DJ (1991) Metabolism of the oral contraceptive steroids ethynylestradiol and norgestimate by normal (Huma 7) and malignant (MCF-7 and ZR-75-1) human breast cells in culture. *J Steroid Biochem Mol Biol* **39**: 535-543.

Wild MJ, Rudland PS, and Back DJ (1993) Metabolism of the oral contraceptive steroids ethynylestradiol, norgestimate and 3-ketodesogestrel by a human endometrial cancer cell line (HEC-1A) and endometrial tissue in vitro. *J Steroid Biochem Mol Biol* **45**: 407-420.

Xu C, and Desta Z (2013) In vitro analysis and quantitative prediction of efavirenz inhibition of eight cytochrome P450 (CYP) enzymes: major effects on CYPs 2B6, 2C8, 2C9 and 2C19. *Drug Metab Pharmacokinet* **28**: 362-371.

Yang X, Atkinson K, and Di L (2016) Novel Cytochrome P450 Reaction Phenotyping for Low-Clearance Compounds Using the Hepatocyte Relay Method. *Drug Metabolism and Disposition* **44**: 460-465.

Zeldin RK, and Petruschke RA (2004) Pharmacological and therapeutic properties of ritonavir-boosted protease inhibitor therapy in HIV-infected patients. *Journal of antimicrobial Chemotherapy* **53**: 4-9.

Zhang D, Chando TJ, Everett DW, Patten CJ, Dehal SS, and Humphreys WG (2005) In vitro inhibition of udp glucuronosyltransferases by atazanavir and other hiv protease inhibitors and the relationship of this property to in vivo bilirubin glucuronidation. *Drug Metabolism and Disposition* **33**: 1729-1739.

Zhang J, Chung E, Yones C, Persson A, Mahnke L, Eley T, Xu X, and Bertz R (2011) The effect of atazanavir/ritonavir on the pharmacokinetics of an oral contraceptive containing ethinyl estradiol and norgestimate in healthy women. *Antivir Ther* **16**: 157-164.

DMD Fast Forward. Published on March 10, 2017 as DOI: 10.1124/dmd.116.073940
This article has not been copyedited and formatted. The final version may differ from this version.

Footnotes

Deepak Ahire and Sarmistha Sinha: Equal contribution

DMD Fast Forward. Published on March 10, 2017 as DOI: 10.1124/dmd.116.073940
This article has not been copyedited and formatted. The final version may differ from this version.

Figure Legends

Figure 1: LC/MS Chromatogram of NGMN and its metabolites after incubating the substrates in NADPH supplemented HLM. Separations were achieved on a Thermo Hypersil Gold C18 column and detected by a LTQ-Velos Orbitrap. The different panels contain the extracted ion chromatograms of parent and various metabolites.

Figure 2: Fragmentation of NGMN after its fragmentation in an LTQ-Velos-Orbitrap using collision induced disassociation fragmentation.

Figure 3: LC/MS Chromatogram of NG and its metabolites after incubating the substrates in NADPH supplemented HLM. Separations were achieved on a Thermo Hypersil Gold C18 column and detected by a LTQ-Velos Orbitrap. The different panels contain the extracted ion chromatograms of parent and various metabolites.

Figure 4: Fragmentation of NG after its fragmentation in an LTQ-Velos-Orbitrap using collision induced disassociation fragmentation.

Figure 5: Metabolic pathway of norgestimate and downstream putative metabolic pathway of NGMN and NG (Met 7) in human liver microsomes.

Figure 6: The first order disappearance of NGMN in the presence of various recombinant CYPs (rCYPs).

Figure 7: Metabolite formation of NGMN in the presence of various recombinant CYPs (rCYPs). Metabolites Met 1, 2, 3, 4, 5 and 6 are shown in panels A, B, C, D, E and F, respectively.

Figure 8: Reaction phenotyping of NGMN in HLM in presence of selective CYP inhibitors. Panel A shows the first order parent disappearance of NGMN while panels B, C, D, E and F show the inhibition in formation of Met 1, 3, 4, 5 and 6, respectively.

Figure 9: Effect of various parameters on the NGMN fold-AUC change for inhibition and induction mediated DDIs of NGMN. While the AUC change is of NGMN (victim), the C_{max}, K_I and k_{inact} are the perpetrator properties as described in Table 1. The values of f_m, k_{inact}, K_I and C_{max} used are 0.57, 0.11 (1/min), 1000 nM and 14.8 μM. Panels A, B, C and D show the effect of f_m, C_{max}, k_{inact} and K_I, respectively.

DMD Fast Forward. Published on March 10, 2017 as DOI: 10.1124/dmd.116.073940
This article has not been copyedited and formatted. The final version may differ from this version.

Table 1: Table of *in vitro* values of perpetrators and NGMN AUC values from clinical studies

	Dose (mg)	**CYP3A4 K_I nM**	**CYP3A4 $k_{inact}(min^{-1})$**	**CYP3A4 K_i (nM)**	**CYP3A4 EC_{50}(µM)**	**CYP3A4 E_{max}**	**NGMN AUC_i pg*h/ml**	**NGMN AUC pg*h/ml**	**Refs**
Lopinavir	400	1000	0.11	7300			138	76	(Weemhoff et al., 2003; Ernest et al., 2005; Fahmi et al., 2008; Vogler et al., 2010)
Ritonavir Study 1	100	170	0.4	40	1000	68.5	138	76	
Atazanavir	300	50	0.049	2300			35022	19188	(Ernest et al., 2005; Fahmi et al., 2008; Hyland et al., 2008; Zhang et al., 2011)
Ritonavir Study 2	100	170	04	40	1000	68.5	35022	19188	
Efavirenz	600	-	-	40000	3900	6.5	6522	18328	(Sevinsky et al., 2011; Siccardi et al., 2013; Xu and Desta, 2013)

K_I is the perpetrator irreversible inhibition constant, k_{inact} the perpetrator maximum irreversible inactivation rate constant; K_i the perpetrator reversible inhibitor constant, EC_{50} the perpetrator concentration of inducer causing half maximal induction, E_{max} is the perpetrator fold induction in enzyme activities, where AUC_i is the NGMN (victim) area under of the plasma concentration versus time curve in the presence of an inhibitor, AUC the NGMN area under of the plasma concentration versus time curve in the absence of an inhibitor

DMD Fast Forward. Published on March 10, 2017 as DOI: 10.1124/dmd.116.073940
This article has not been copyedited and formatted. The final version may differ from this version.

Table 2: Metabolite Profile of NGMN after incubation of 30 μM NGMN in 1 mM NADPH supplemented 1 mg/ml HLM

Parent/Metabolites	**RT**	**MH^+**	**% relative abundance (UV)**
NGMN	28.31	328.2271	83.0
Met1	15.77	344.222	1.5
Met2	16.55	360.2169	2.0
Met3	19.49	344.222	2.0
Met4	21.35	344.222	3.0
Met5	24.14	344.222	2.0
Met6	26.47	344.222	1.5
Met7/NG	27.02	313.2162	5.0

DMD Fast Forward. Published on March 10, 2017 as DOI: 10.1124/dmd.116.073940
This article has not been copyedited and formatted. The final version may differ from this version.

Table 3: Metabolite Profile of NG after incubation of 30 μM NG in 1 mM NADPH supplemented 1 mg/ml HLM

Parent/Metabolites	**RT**	**MH^+**	**% relative abundance (UV)**
NG	27.04	313.2162	88.0
Met8	17.94	329.2111	2.0
Met9	18.63	489.2483	6.0
Met10	20.74	329.2111	1.0
Met11			
Met12	21.16	329.2111	1.0
Met13	22.05	329.2111	1.0
Met14	22.36	329.2111	1.0

Table 4:

Retrospectively determined predicted and observed AUC changes of NGMN from clinical trials. The perpetrator *in vitro* values shown in Table 3 were used for the DDI predictions. Equations 2 to 4, as defined in the methods section, were used to calculate the fold changes in AUC. Lopinavir (LPR) and Ritonavir (RTV) were co-administered in one study (Vogler et al., 2010), while atazanavir and ritonavir were co-administered in another study (Zhang et al., 2011). Hence, the fold AUC changes are the same for LPR and RTV (study 1), and for ATV and RTV (study 2).Efavirenz was dosed in a separate study (Sevinsky et al., 2011)

Perpetrator conc.Paradigm	Perpetrator (Dose, mg)	Perpetrator conc., nM	NGMN Predicted AUCi/AUC	NGMN Observed AUCi/AUC	Ratio of predicted/observed
Total C_{max}	Lopinavir (400)	14790	2.3	1.82	1.28
Free C_{max}	Lopinavir (400)	118	2.2	1.82	1.24
I_h	Lopinavir (400)	42526	2.3	1.82	1.28
Total C_{max}	Ritonavir, study 1 (100)	745	2.3	1.82	1.28
Free C_{max}	Ritonavir, study 1 (100)	2	2.1	1.82	1.17
I_h	Ritonavir, study 1 (100)	9249	2.3	1.82	1.28
Total C_{max}	Atazanavir (300)	9616	2.3	1.83	1.27

DMD Fast Forward. Published on March 10, 2017 as DOI: 10.1124/dmd.116.073940
This article has not been copyedited and formatted. The final version may differ from this version.

Free C_{max}	Atazanavir (300)	1298	2.3	1.83	1.26
I_h	Atazanavir (300)	29667	2.3	1.83	1.27
Total C_{max}	Ritonavir, study 2 (100)	2053	2.3	1.83	1.27
Free C_{max}	Ritonavir, study 2 (100)	6	2.3	1.83	1.27
I_h	Ritonavir, study 2 (100)	9253	2.3	1.83	1.27
Total C_{max}	Efavirenz (600)	21161	0.4	0.36	0.98
Free C_{max}	Efavirenz (600)	127	0.9	0.36	2.49
I_h	Efavirenz (600)	126842	0.7	0.36	1.94

DMD Fast Forward. Published on March 10, 2017 as DOI: 10.1124/dmd.116.073940
This article has not been copyedited and formatted. The final version may differ from this version.

Figure 1:

Figure 1

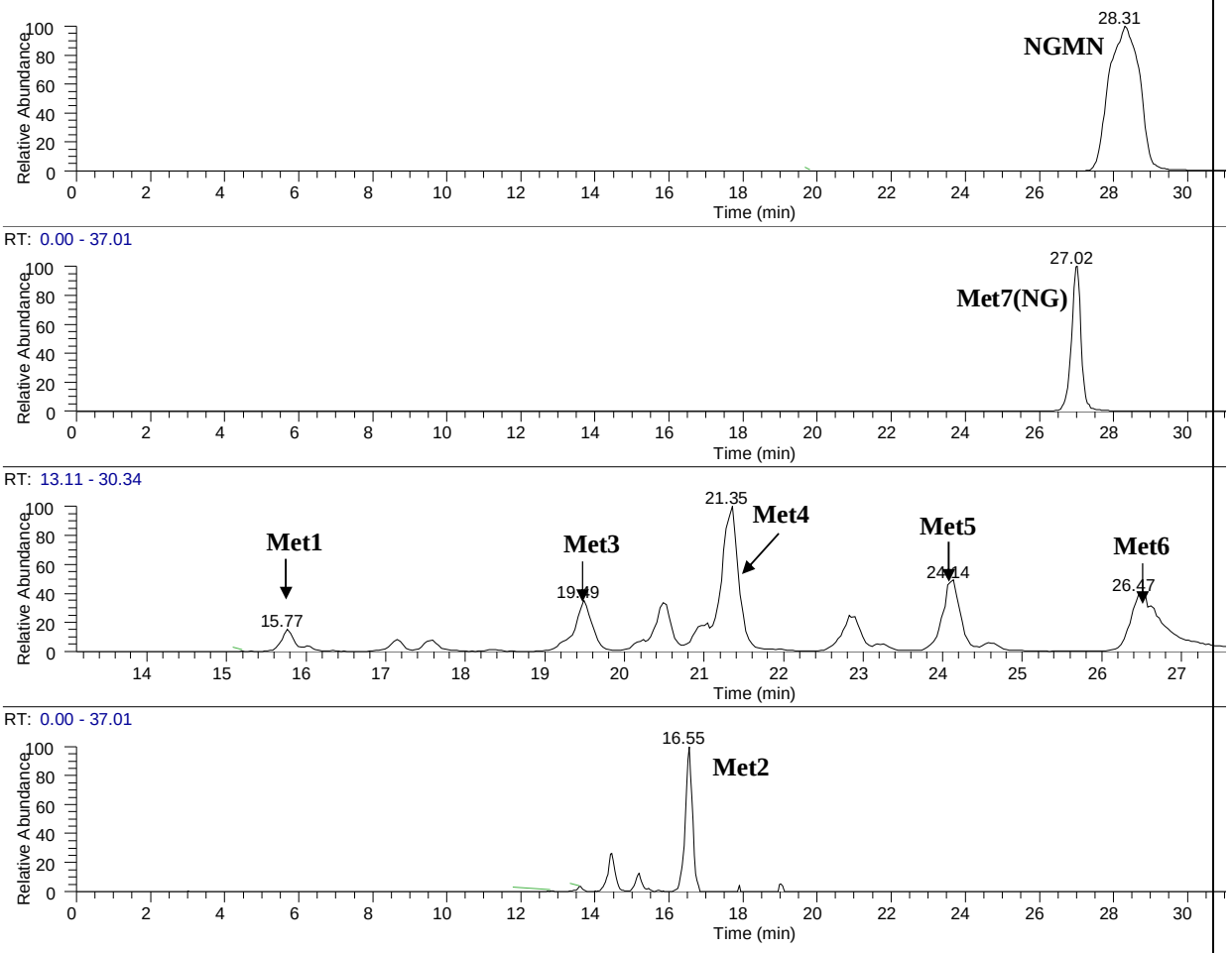

Figure 2

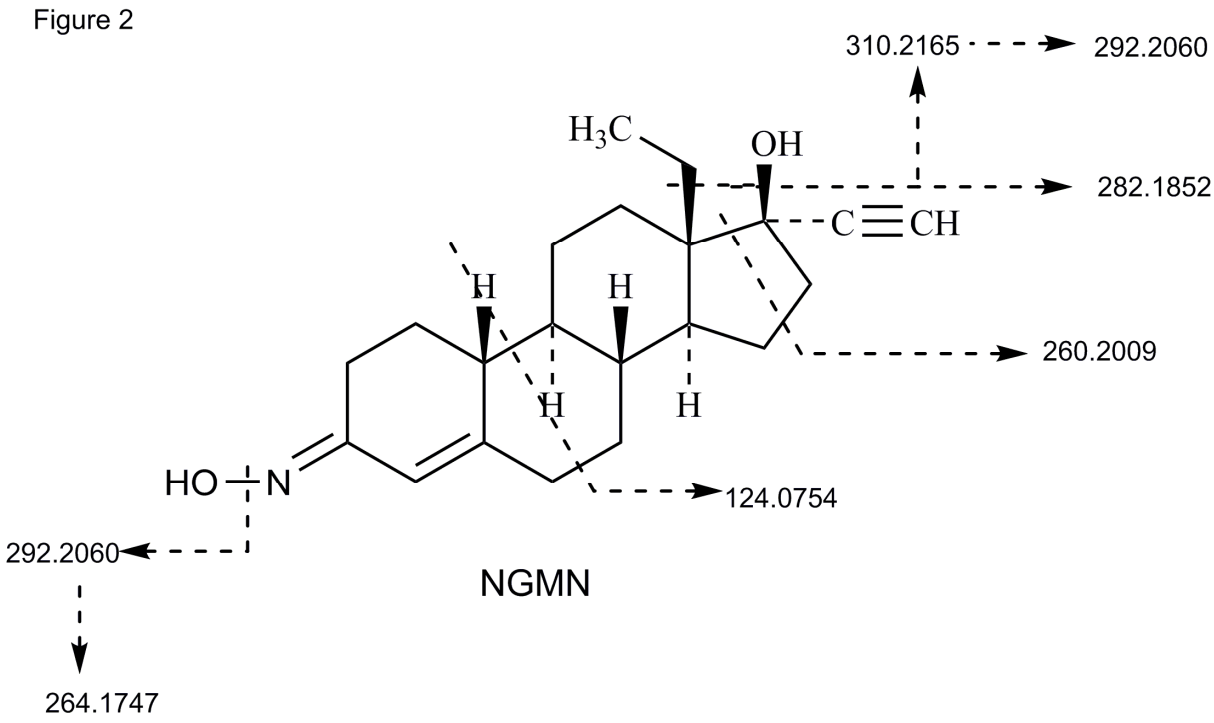

DMD Fast Forward. Published on March 10, 2017 as DOI: 10.1124/dmd.116.073940
This article has not been copyedited and formatted. The final version may differ from this version.

Figure 3

Figure 3

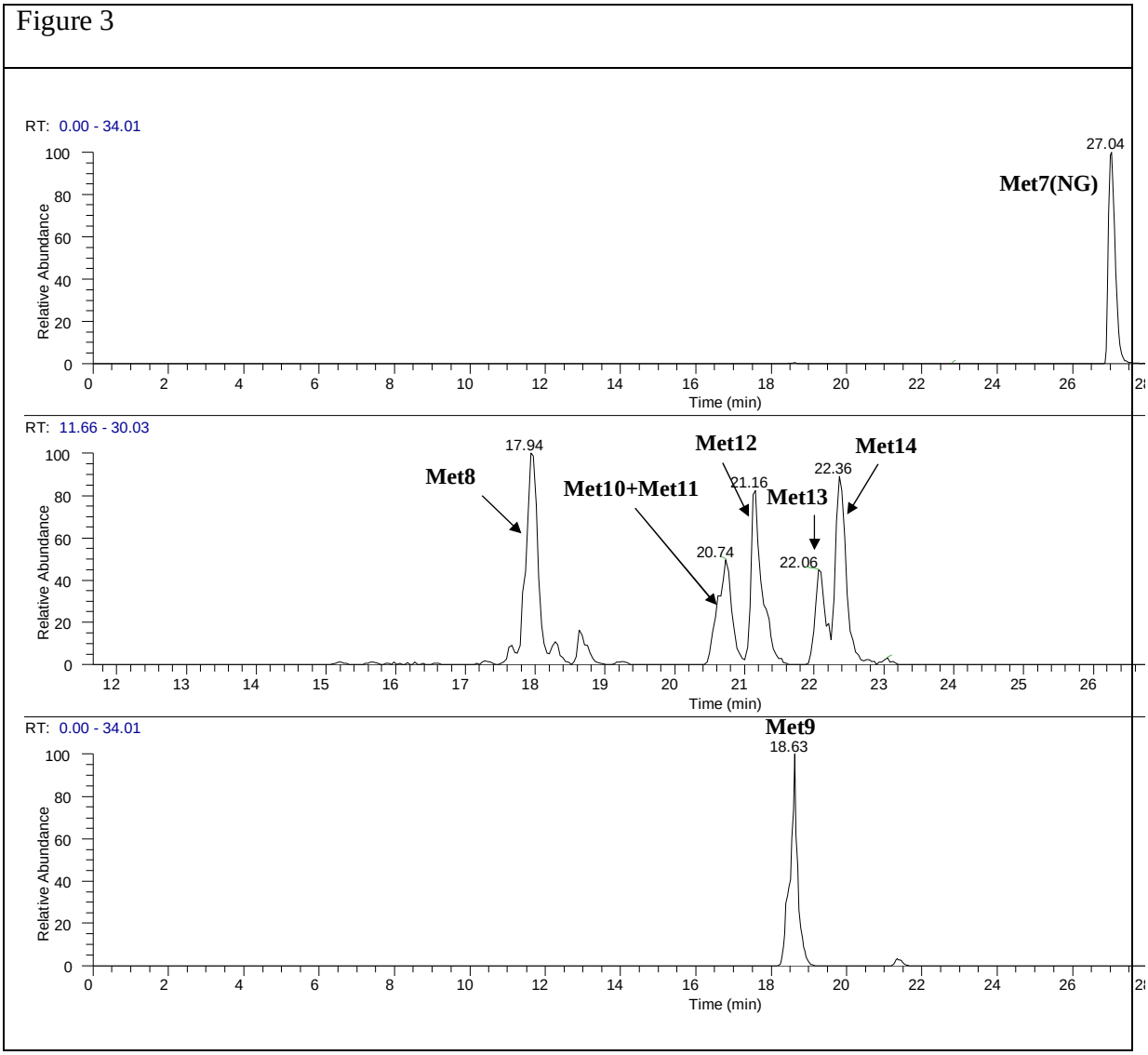

DMD Fast Forward. Published on March 10, 2017 as DOI: 10.1124/dmd.116.073940
This article has not been copyedited and formatted. The final version may differ from this version.

Figure 4

Figure 4

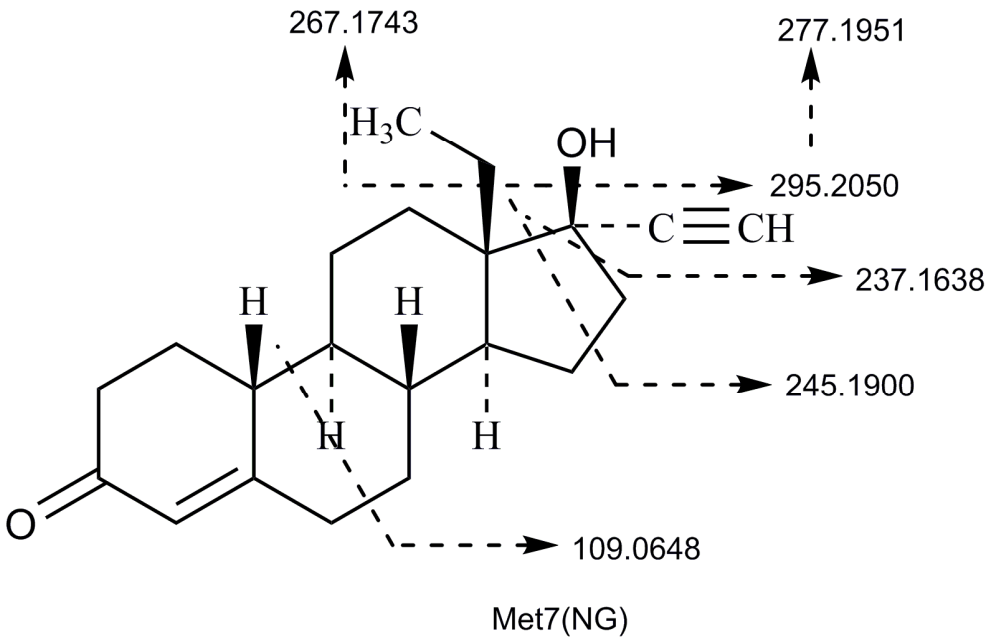

DMD Fast Forward. Published on March 10, 2017 as DOI: 10.1124/dmd.116.073940
This article has not been copyedited and formatted. The final version may differ from this version.

Figure 5

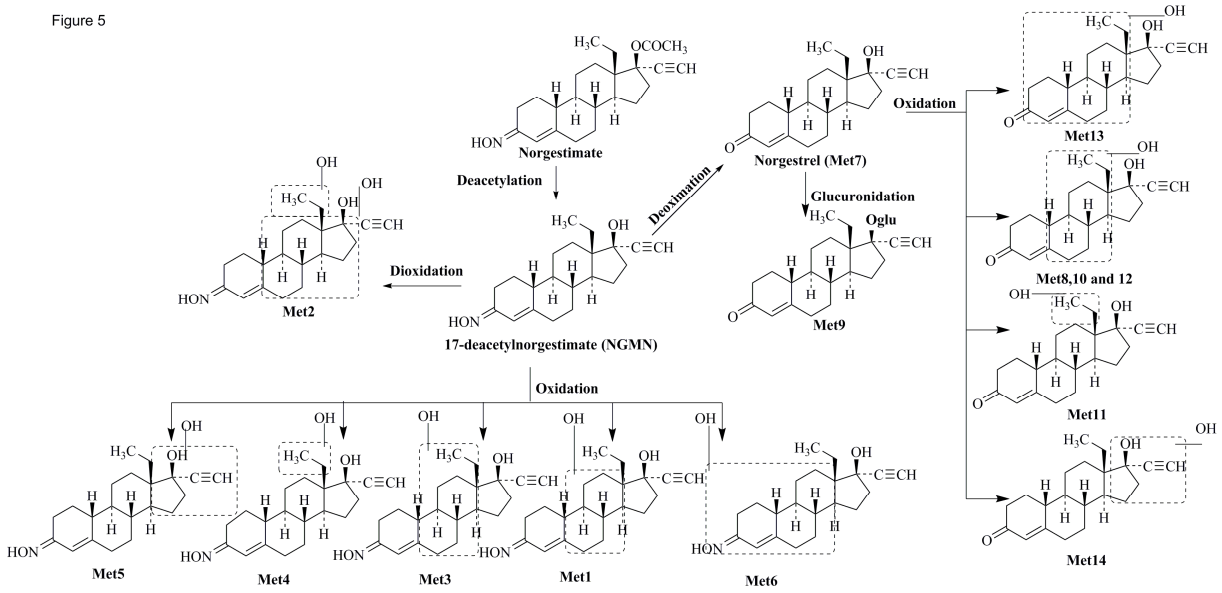

DMD Fast Forward. Published on March 10, 2017 as DOI: 10.1124/dmd.116.073940
This article has not been copyedited and formatted. The final version may differ from this version.

Figure 6

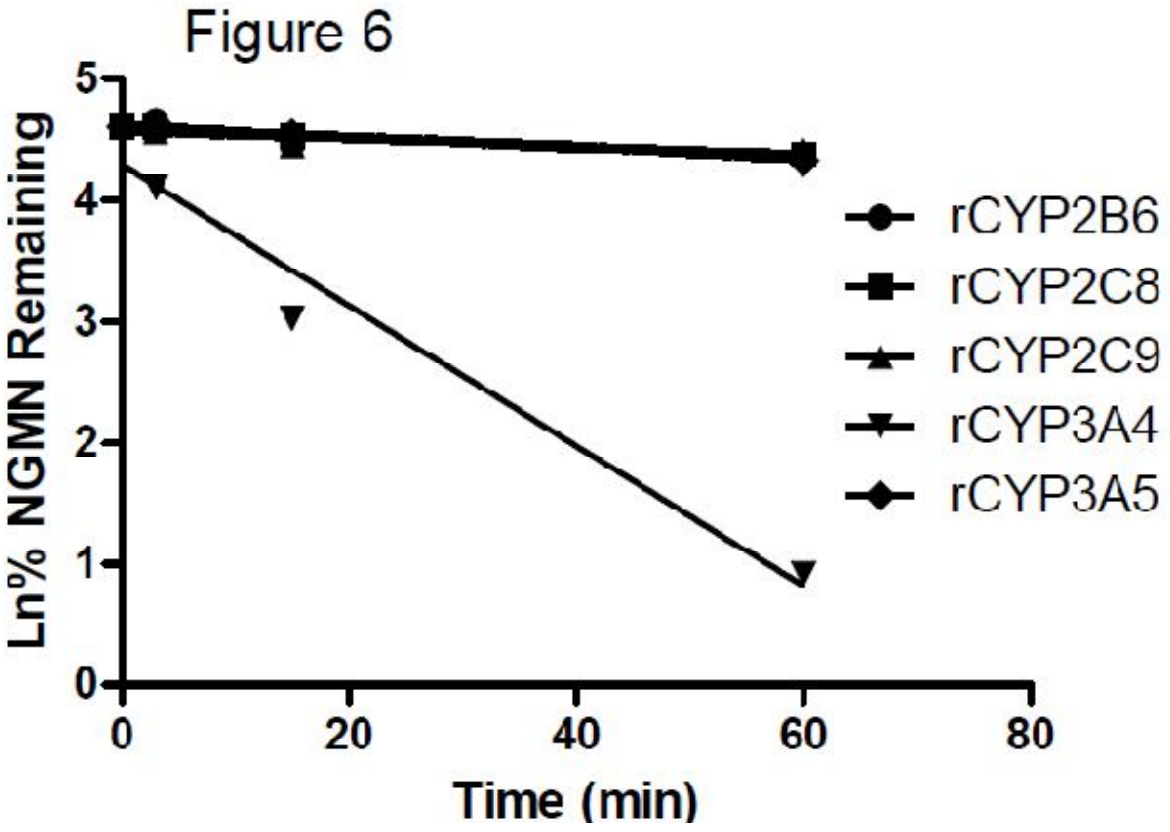

DMD Fast Forward. Published on March 10, 2017 as DOI: 10.1124/dmd.116.073940
This article has not been copyedited and formatted. The final version may differ from this version.

Figure 7

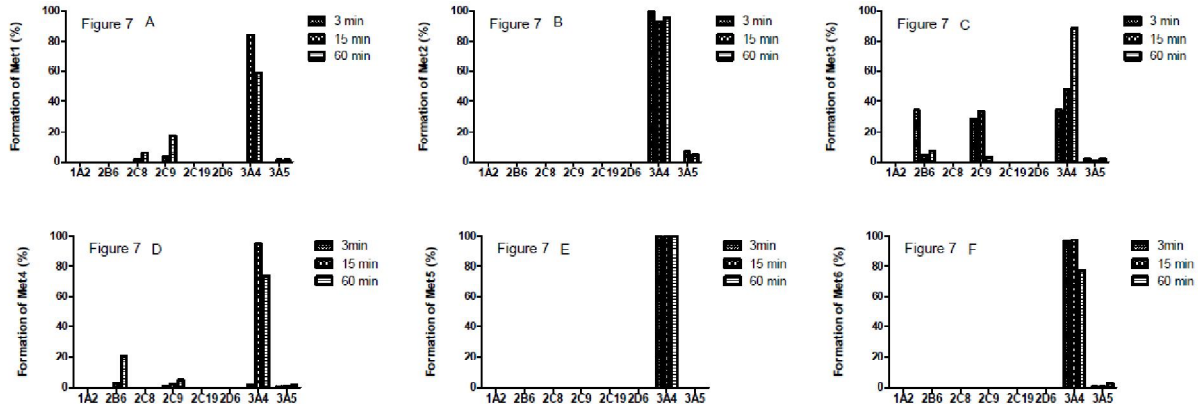

DMD Fast Forward. Published on March 10, 2017 as DOI: 10.1124/dmd.116.073940
This article has not been copyedited and formatted. The final version may differ from this version.

Figure 8

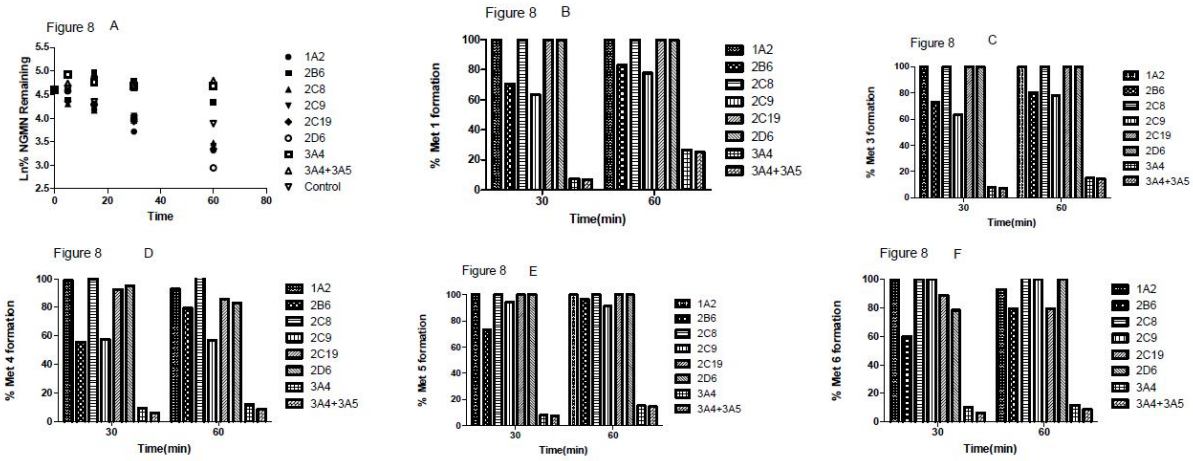

DMD Fast Forward. Published on March 10, 2017 as DOI: 10.1124/dmd.116.073940
This article has not been copyedited and formatted. The final version may differ from this version.

Figure 9

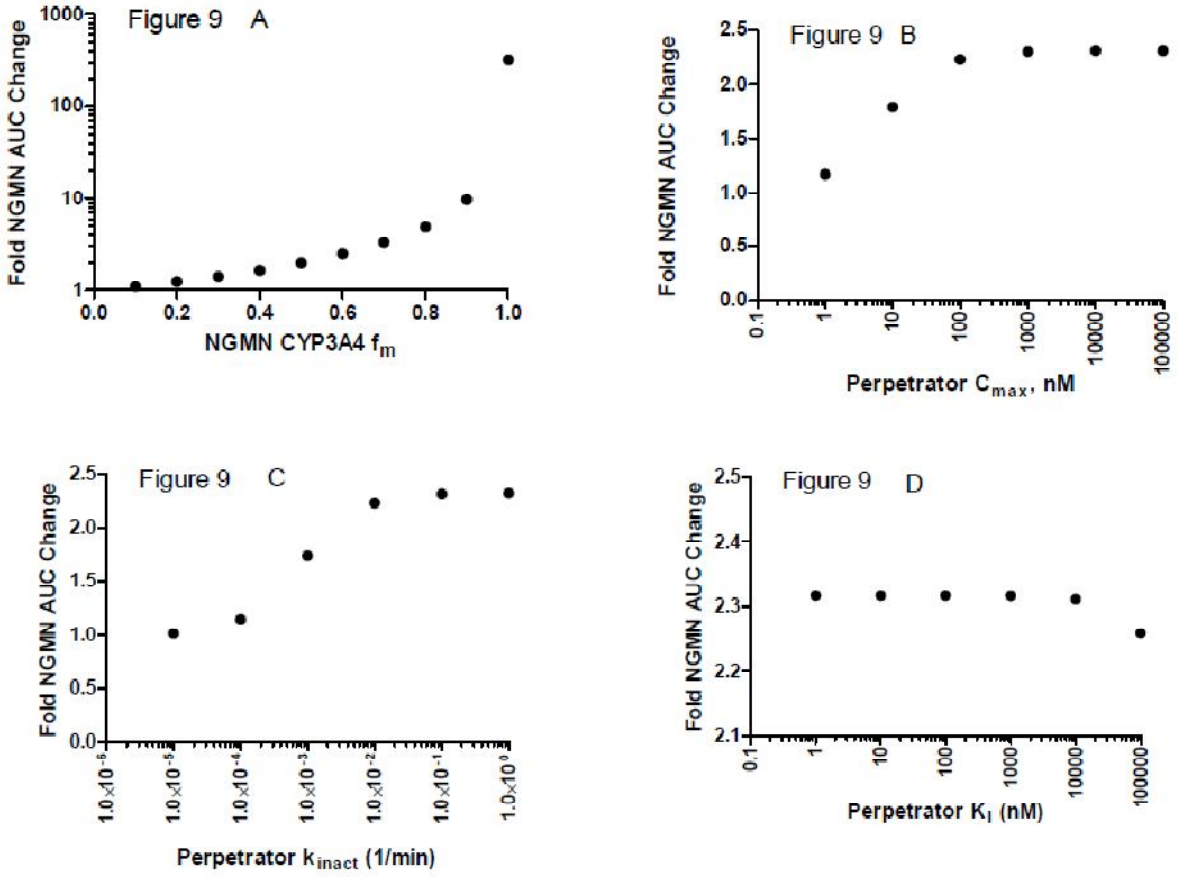

Metabolite Identification, Reaction Phenotyping and Retrospective Drug-Drug Interaction Predictions of 17-deacetylnorgestimate, the Active Component of the Oral Contraceptive Norgestimate

Deepak Ahire, Sarmistha Sinha, Barry Brock, Ramaswamy Iyer, Sandhya Mandlekar and Murali Subramanian

Submitted to: Drug Metabolism and Disposition; **DMD/2016/073940**

Supplementary Figure 1: Disappearance of NGMN in all tested recombinant cytochrome P450s (A) and NG in all the tested recombinant cytochrome P450s (B) and UGTs (C)

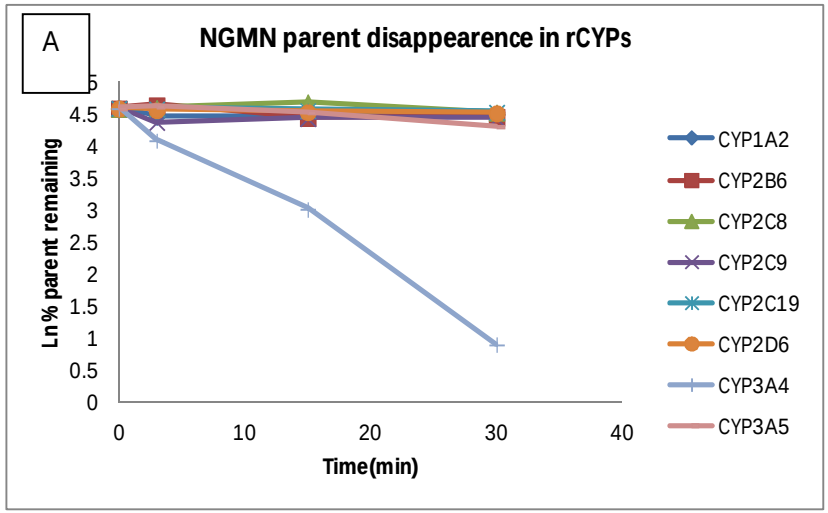

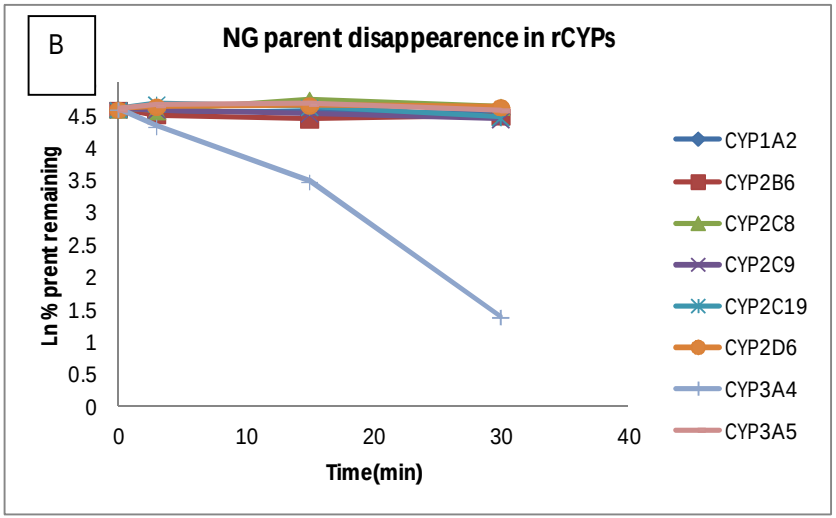

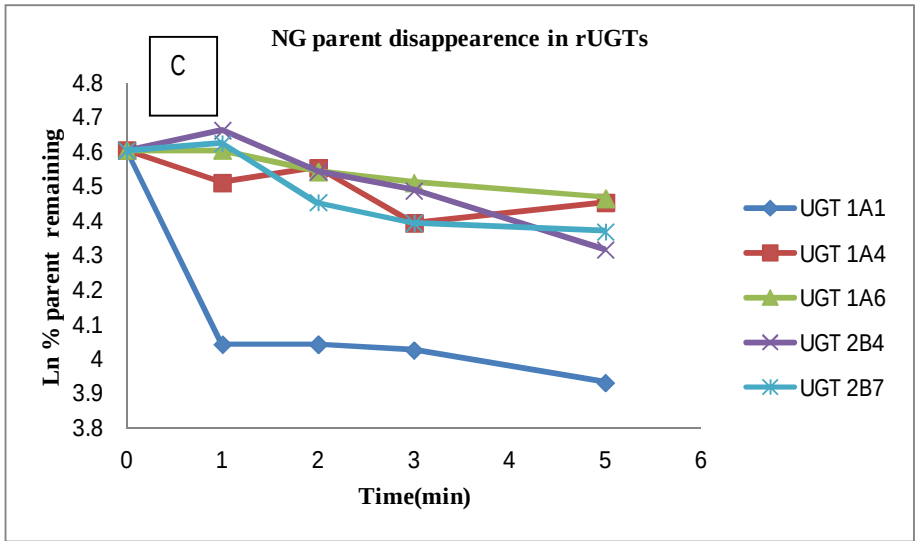

Supplementary Figure 2: HRMS spectra of NGMN along with structure elucidation of metabolites. Panel A, B, C, D, E, F, G and H show the spectra and fragmentation for NGMN, Met 1, Met 2, Met 3, Met 4, Met 5, Met 6 and Met 7 (NG), respectively.

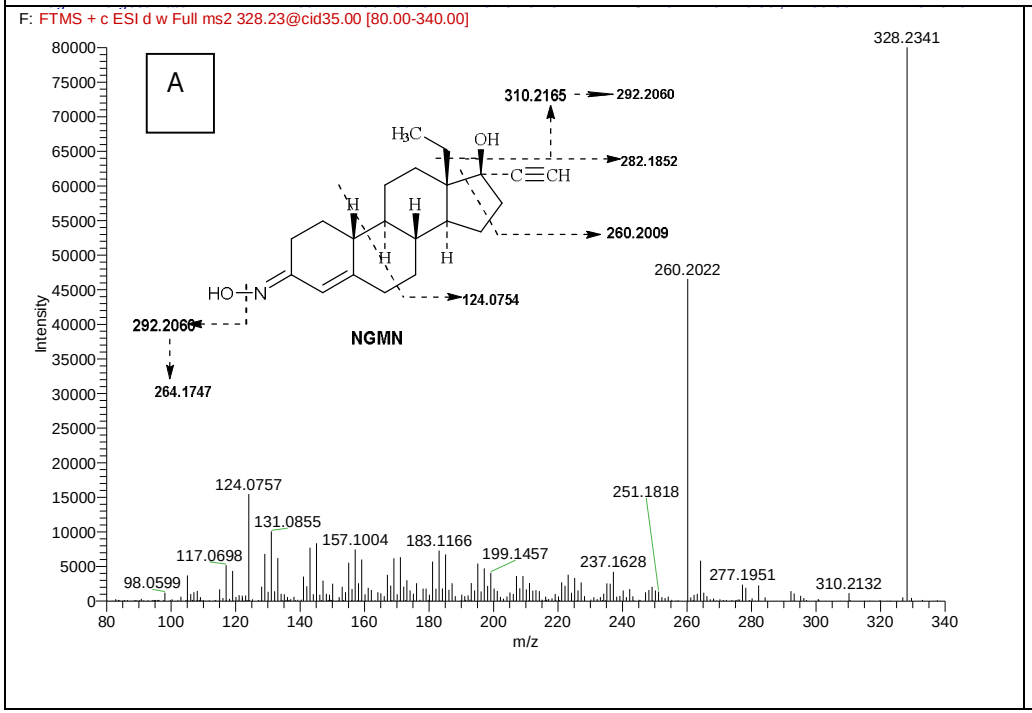

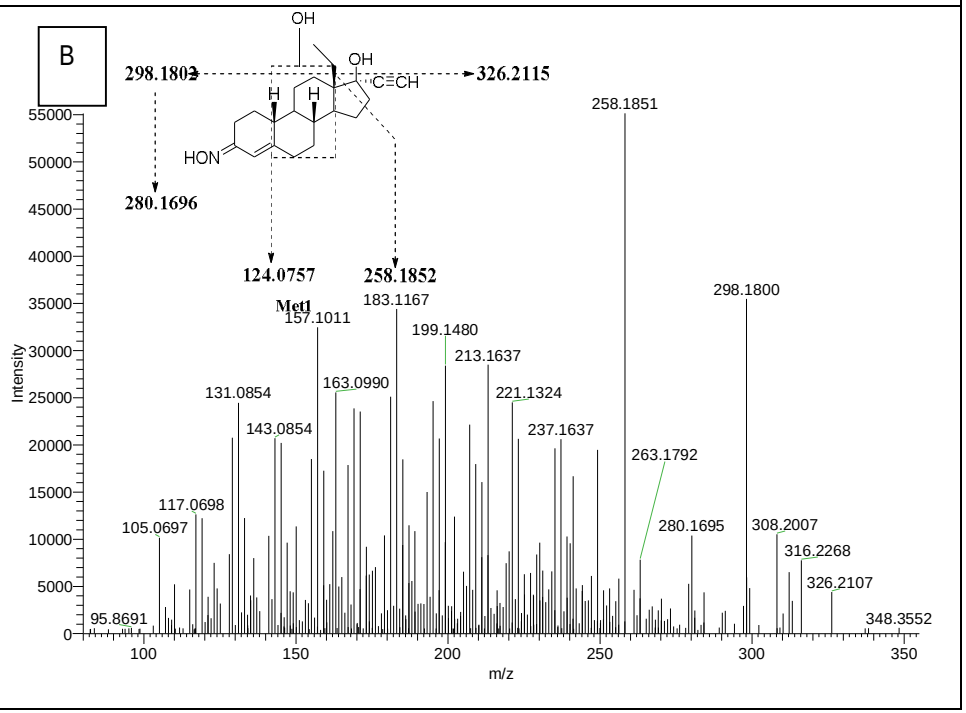

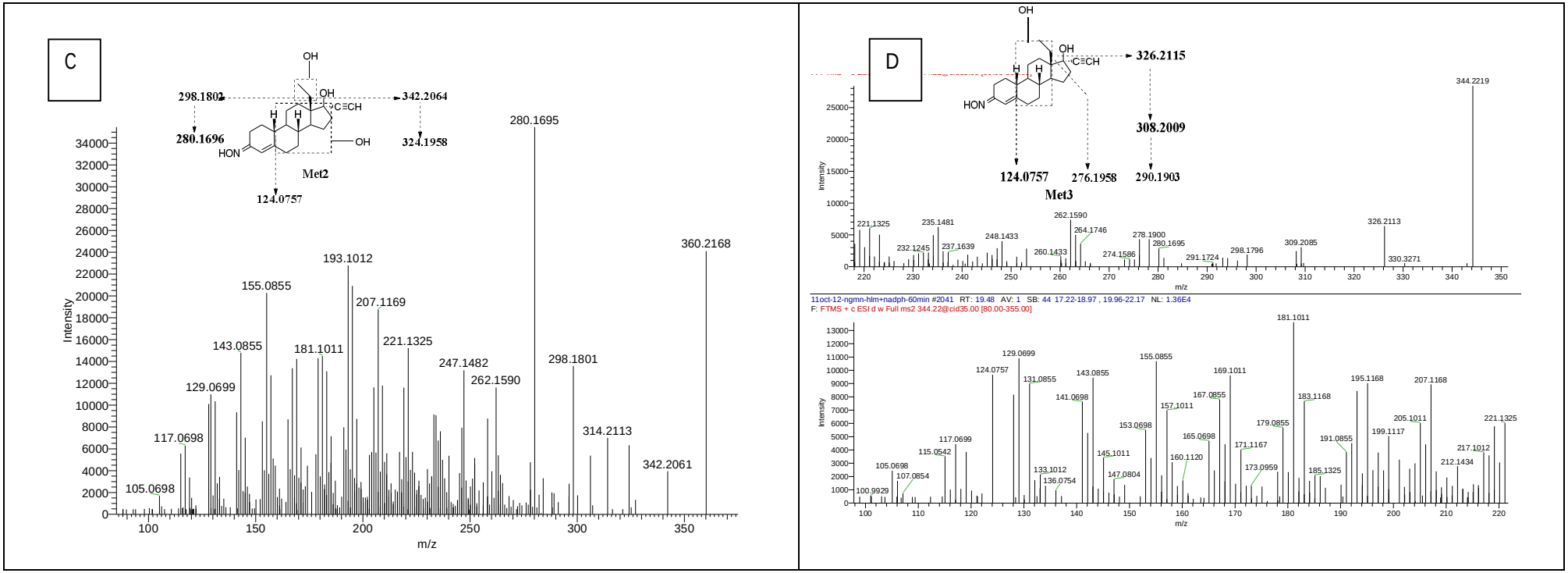
C
OH
OH
C≡CH
H
H
HON
OH
298.1802
342.2064
280.1696
324.1958
124.0757
Met2
280.1695
360.2168
193.1012
155.0855
207.1169
143.0855
181.1011
221.1325
247.1482
262.1590
298.1801
129.0699
314.2113
117.0698
342.2061
105.0698
Intensity
m/z
D
OH
OH
C≡CH
H
H
HON
326.2115
308.2009
124.0757
276.1958
290.1903
Met3
344.2219
221.1325
235.1481
262.1590
264.1746
248.1433
278.1900
280.1695
232.1245
237.1639
260.1433
274.1586
291.1724
298.1796
309.2085
326.2113
330.3271
Intensity
m/z
11oct-12-ngmn-hlm+nadph-60min #2041 RT: 19.48 AV: 1 SB: 44 17.22-18.97 , 19.96-22.17 NL: 1.36E4
F: FTMS + c ESI d w Full ms2 344.22@cid35.00 [80.00-355.00]
181.1011
129.0699
124.0757
131.0855
143.0855
155.0855
169.1011
141.0698
167.0855
157.1011
183.1168
195.1168
207.1168
153.0698
179.0855
205.1011
165.0698
171.1167
199.1117
221.1325
117.0699
115.0542
191.0855
160.1120
145.1011
217.1012
105.0698
107.0854
173.0959
212.1434
133.1012
136.0754
147.0804
185.1325
100.9929
Intensity
m/z

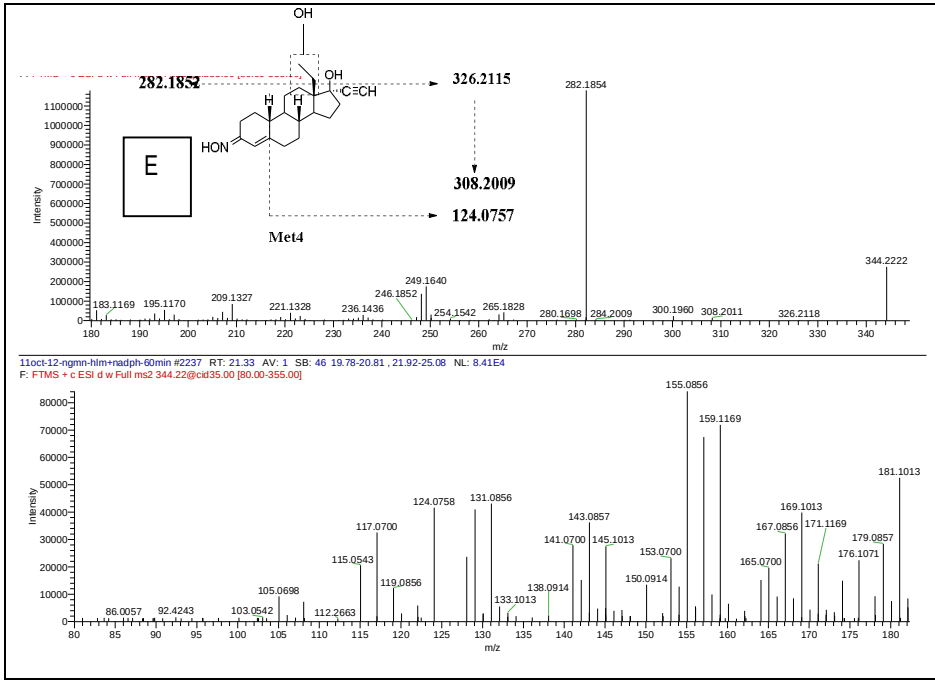
E
OH
OH
C≡CH
H
H
HON
282.1852
326.2115
308.2009
124.0757
Met4
Intensity
m/z
344.2222
249.1640
246.1852
282.1854
183.1169
195.1170
209.1327
221.1328
236.1436
254.1542
265.1828
280.1698
284.2009
300.1960
308.2011
326.2118
11oct-12-ngmn-hlm+nadph-60min #2237 RT: 21.33 AV: 1 SB: 46 19.78-20.81 , 21.92-25.08 NL: 8.41E4
F: FTMS + c ESI d w Full ms2 344.22@cid35.00 [80.00-355.00]
155.0856
159.1169
181.1013
124.0758
131.0856
117.0700
143.0857
169.1013
167.0856
171.1169
141.0700
145.1013
153.0700
179.0857
115.0543
176.1071
165.0700
119.0856
150.0914
105.0698
138.0914
133.1013
86.0057
92.4243
103.0542
112.2663

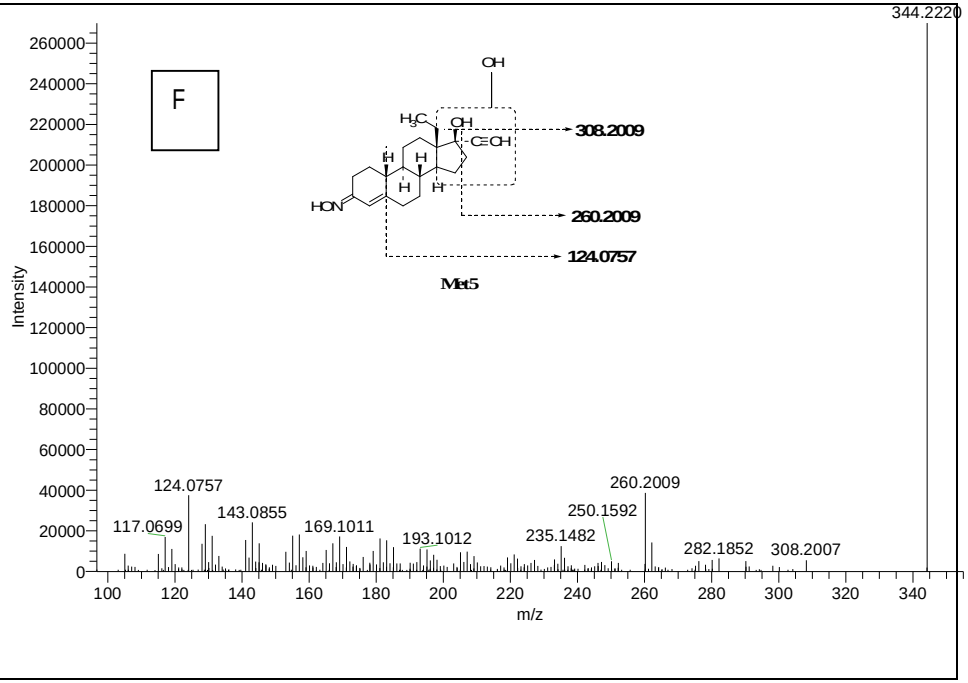
F
OH
H3C
OH
C≡CH
H
H
H
H
HON
308.2009
260.2009
124.0757
Met5
Intensity
m/z
344.2220
124.0757
260.2009
143.0855
250.1592
117.0699
169.1011
193.1012
235.1482
282.1852
308.2007

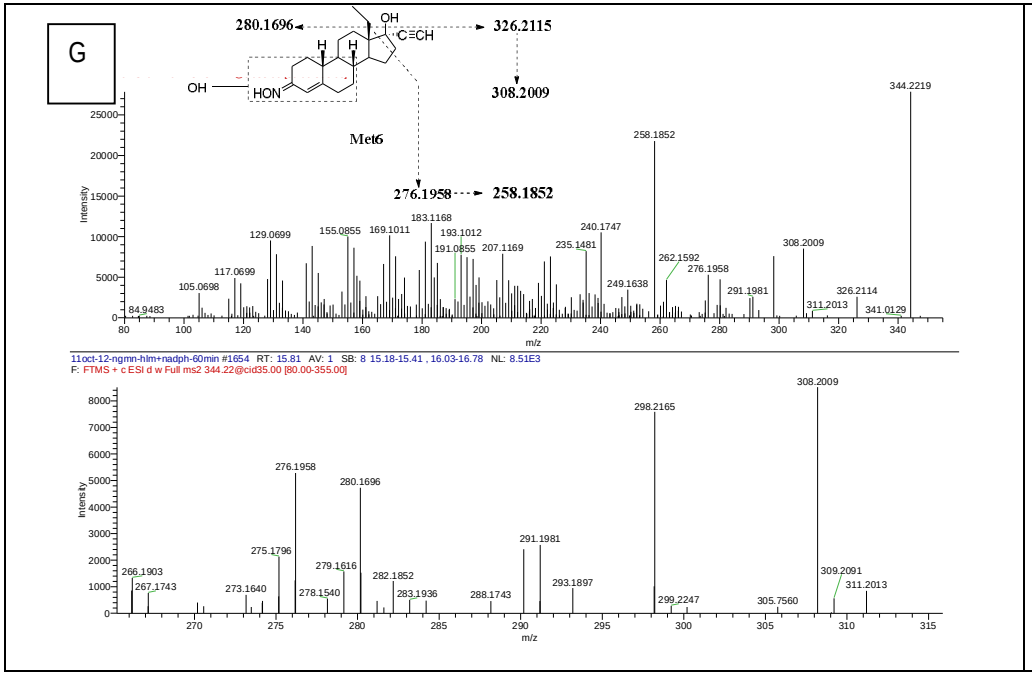
G
280.1696
326.2115
308.2009
276.1958
258.1852
Met6
Intensity
m/z
11oct-12-ngmn-hlm+nadph-60min #1654 RT: 15.81 AV: 1 SB: 8 15.18-15.41 , 16.03-16.78 NL: 8.51E3
F: FTMS + c ESI d w Full ms2 344.22@cid35.00 [80.00-355.00]

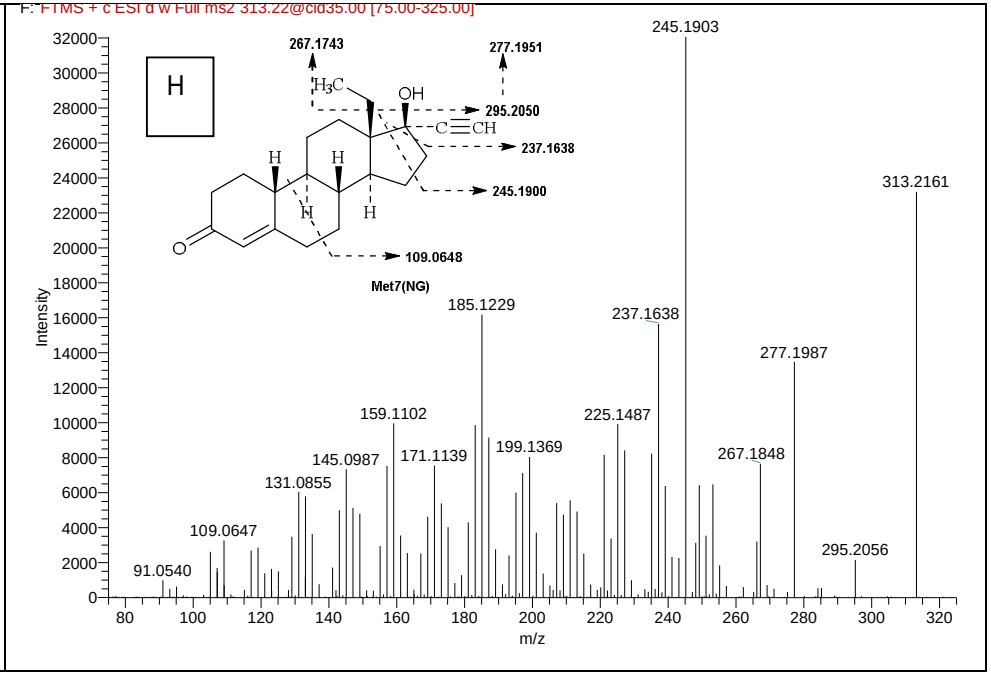
F: FTMS + c ESI d w Full ms2 313.22@cid35.00 [75.00-325.00]
H
267.1743
277.1951
295.2050
237.1638
245.1900
109.0648
Met7(NG)
Intensity
m/z

Supplementary Figure3: HRMS spectra of NG along with structure elucidation of metabolites. Panel A, B, C, D, E, F and G show the spectra and fragmentation for Met 8, Met 9, Met 10, Met 11, Met 12, Met 13 and Met 14, respectively.

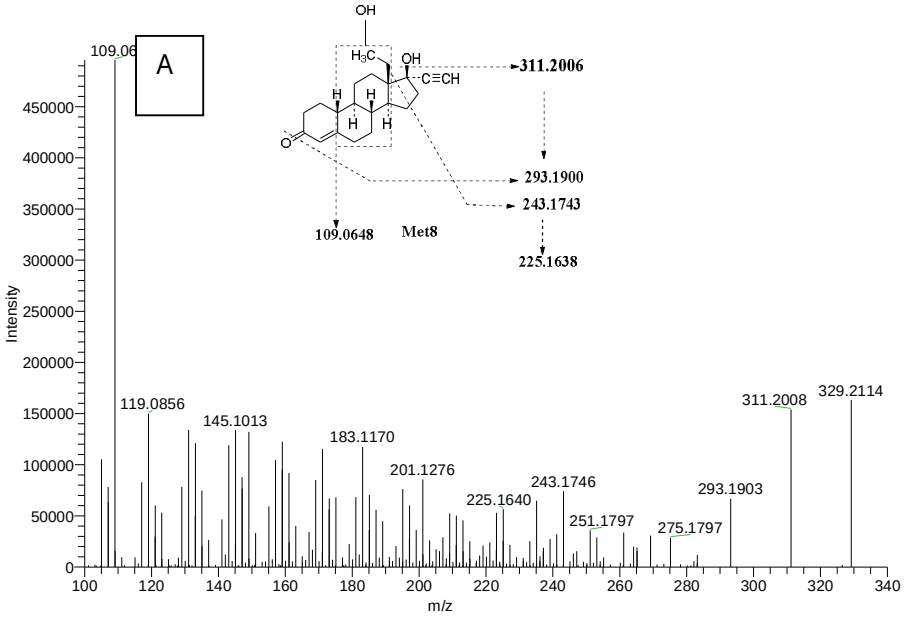

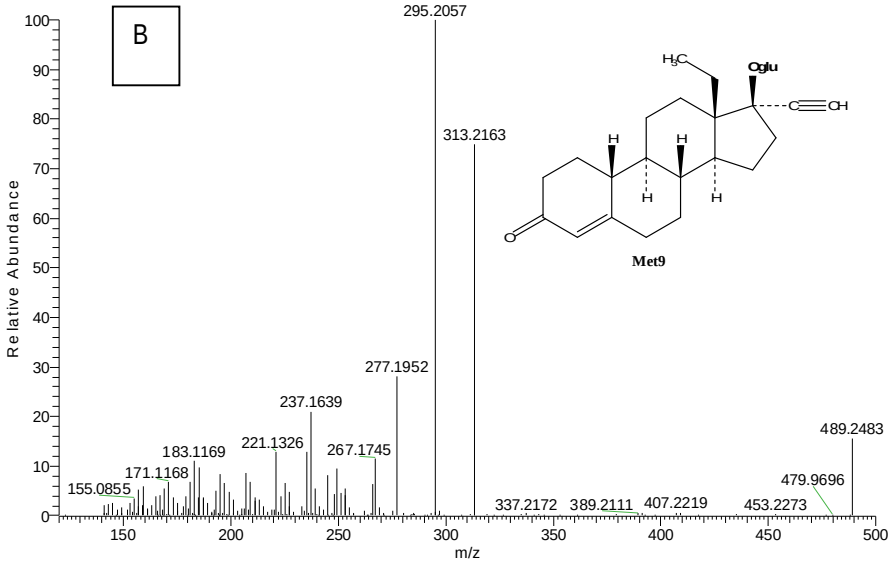

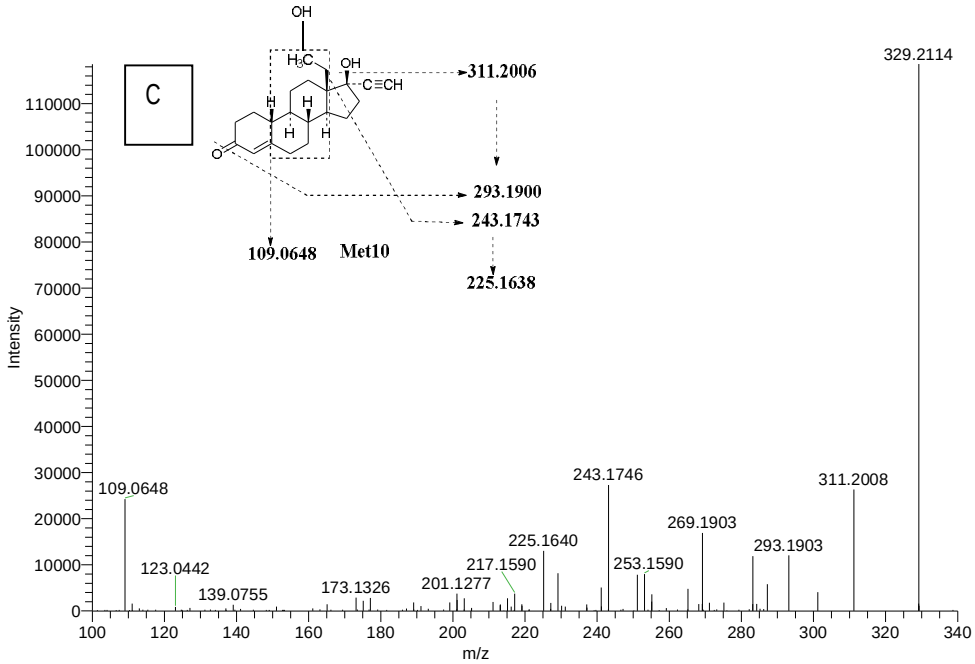
C
OH
H3C
OH
C≡CH
311.2006
293.1900
243.1743
109.0648
Met10
225.1638
Intensity
m/z
329.2114
109.0648
243.1746
311.2008
269.1903
225.1640
293.1903
123.0442
217.1590
253.1590
139.0755
173.1326
201.1277

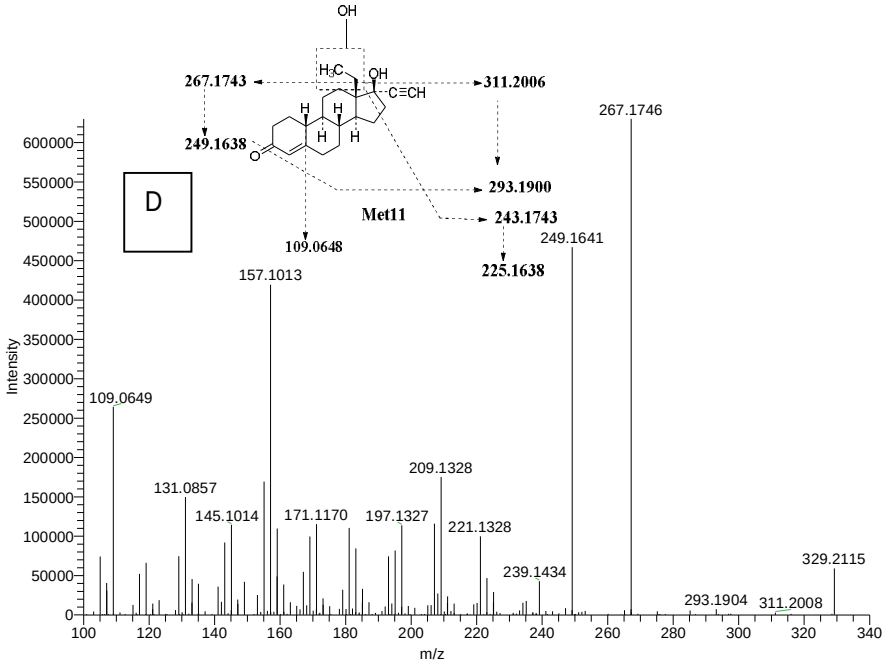
D
OH
H3C
OH
C≡CH
267.1743
311.2006
249.1638
293.1900
Met11
243.1743
109.0648
225.1638
Intensity
m/z
267.1746
249.1641
157.1013
109.0649
209.1328
131.0857
145.1014
171.1170
197.1327
221.1328
239.1434
329.2115
293.1904
311.2008

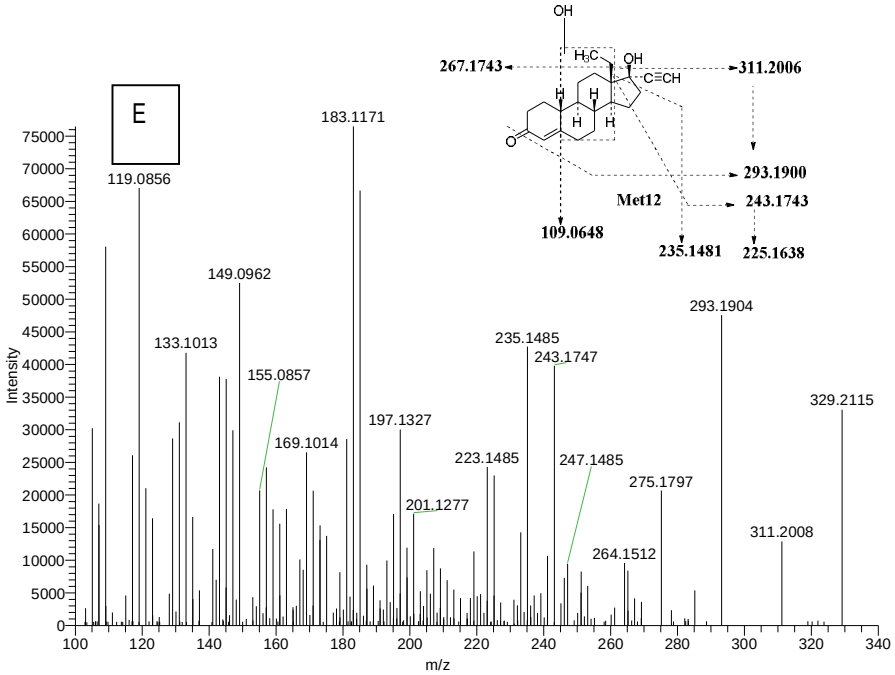
E
OH
H3C
OH
C≡CH
267.1743
311.2006
293.1900
243.1743
Met12
109.0648
235.1481
225.1638
119.0856
183.1171
149.0962
133.1013
293.1904
235.1485
243.1747
155.0857
329.2115
197.1327
169.1014
223.1485
247.1485
275.1797
201.1277
311.2008
264.1512
Intensity
m/z

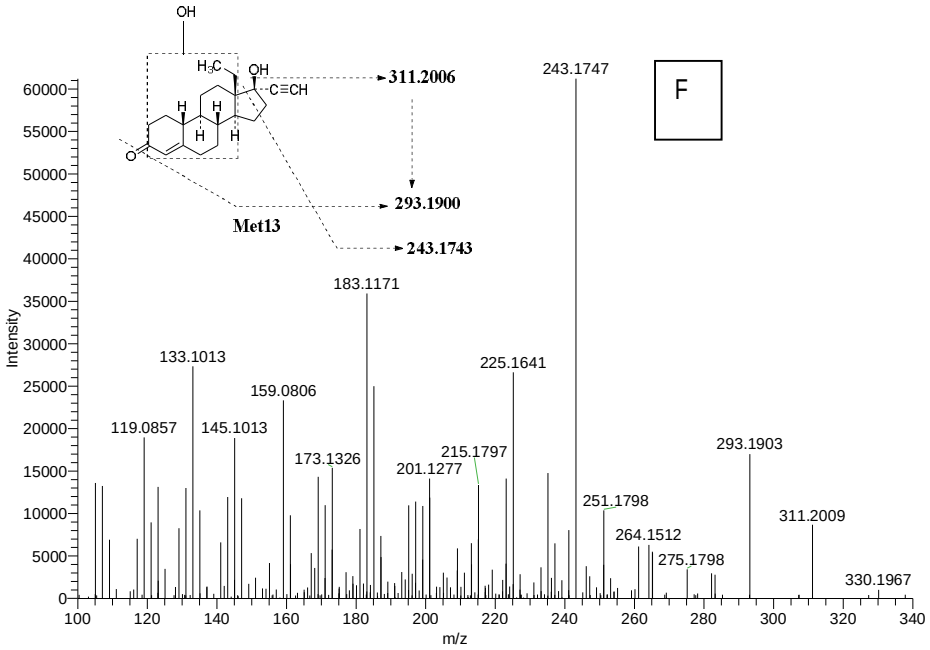
F
OH
H3C
OH
C≡CH
311.2006
243.1747
293.1900
Met13
243.1743
183.1171
133.1013
225.1641
159.0806
119.0857
145.1013
173.1326
215.1797
201.1277
293.1903
251.1798
311.2009
264.1512
275.1798
330.1967
Intensity
m/z

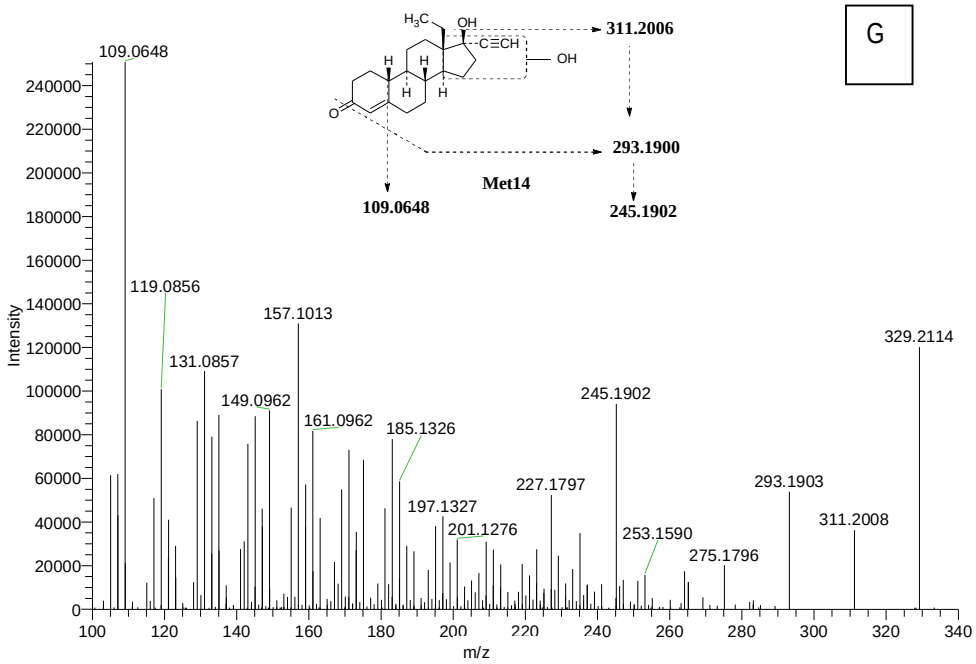
G
H3C
OH
C≡CH
OH
H
H
H
H
O
311.2006
293.1900
Met14
109.0648
245.1902
109.0648
119.0856
157.1013
131.0857
149.0962
161.0962
185.1326
245.1902
329.2114
227.1797
293.1903
197.1327
311.2008
201.1276
253.1590
275.1796
Intensity
m/z
0
20000
40000
60000
80000
100000
120000
140000
160000
180000
200000
220000
240000
100
120
140
160
180
200
220
240
260
280
300
320
340

Supplementary Figure 4: Reaction phenotyping of NG in rCYPs showing % metabolite formation in respective CYP isoform

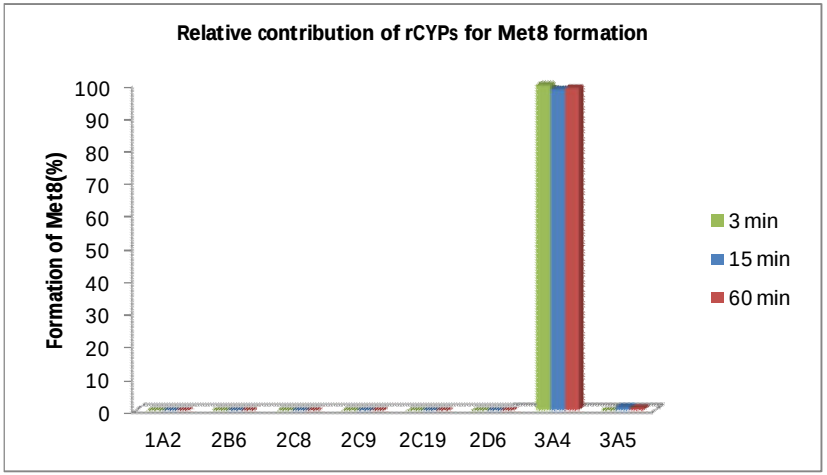

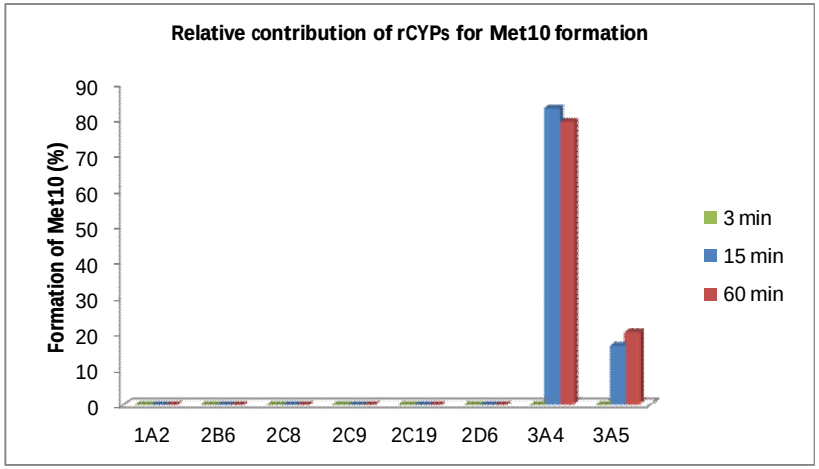

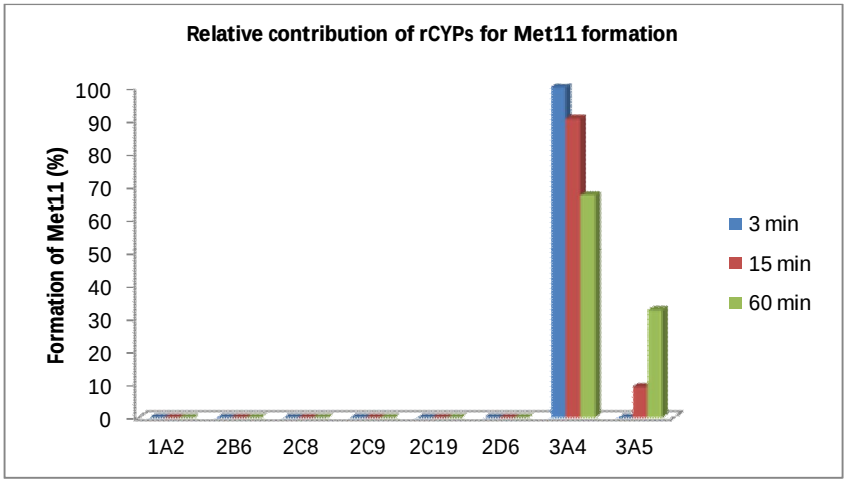

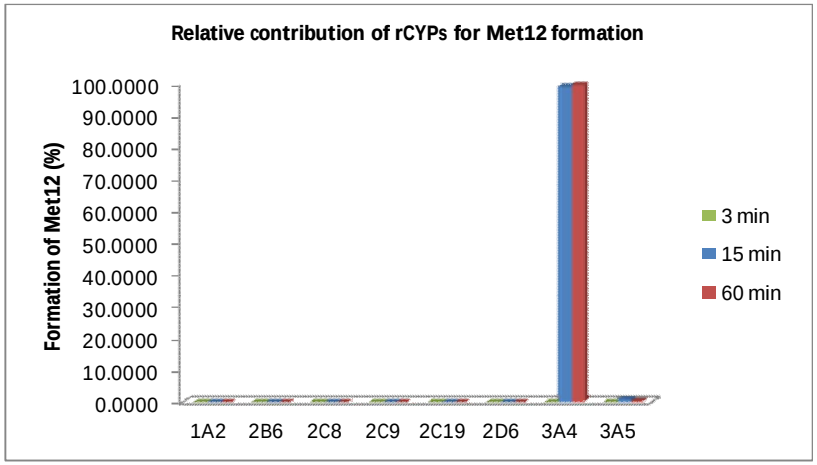

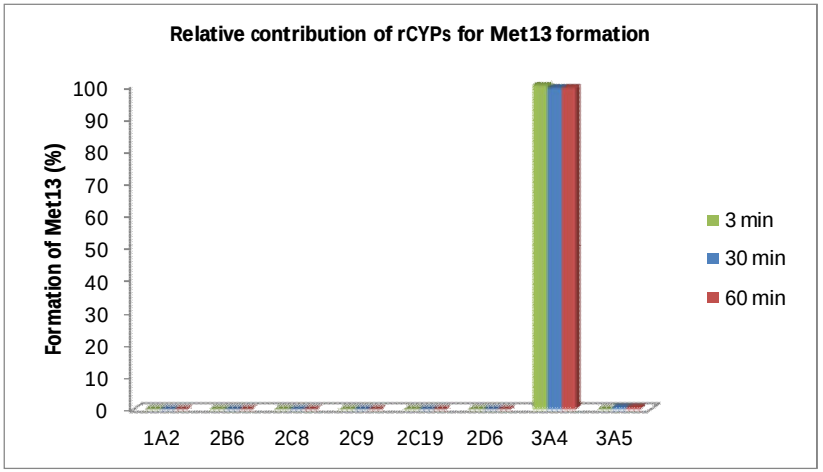
Relative contribution of rCYPs for Met13 formation
Formation of Met13 (%)
100
90
80
70
60
50
40
30
20
10
0
1A2
2B6
2C8
2C9
2C19
2D6
3A4
3A5
3 min
30 min
60 min

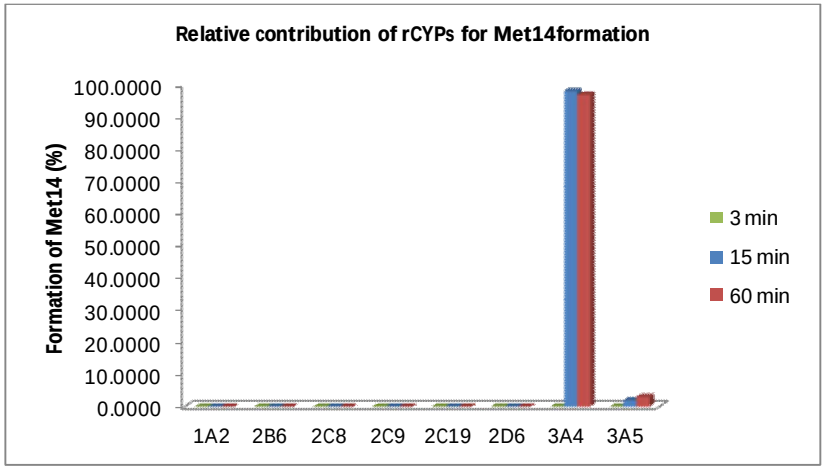
Relative contribution of rCYPs for Met14formation
Formation of Met14 (%)
100.0000
90.0000
80.0000
70.0000
60.0000
50.0000
40.0000
30.0000
20.0000
10.0000
0.0000
1A2
2B6
2C8
2C9
2C19
2D6
3A4
3A5
3 min
15 min
60 min

LC-MS Analysis

LC-MS analysis was carried out using an Agilent 1100 HPLC connected to an Agilent photodiode array detector and an LTQ Velos Orbitrap mass spectrometer fitted with an electrospray ionization probe and operated in the positive-ion mode. Chromatographic separations were performed on a Thermo Hypersil Gold - C18 (150×3 mm; 5 microns) column maintained at 40^{o}C temperature. The mobile phase consisted of solvent A (0.1% formic acid in water) and solvent B (methanol) delivered at a flow rate of 0.4 ml/min with a linear gradient as follows: 5% to 50% B over 12 min, 50% to 70% B from 12 to 28 min, decreased to 5% B from 28 to 47 min. Nitrogen was used as both the sheath gas and auxiliary gas, while helium was used for collision-induced dissociation. The capillary temperature and source voltage were set to 300°C and 5kV, respectively. The orbitrap was operated in Fourier transform mass spectrometry mode to enable the acquisition of both full-scan mass spectra and product-ion MS/MS spectra with mass accuracies within 5 ppm. A typical data-dependent MS method included three scan events: (1) full-scan MS over the range of *m/z* 100-800; (2) MS^2 of the most intense ions exceeding 1000 cps in the previous full-scan mass spectrum; and (3) MS^3 of the most intense product ion from the MS^2 scan. Dynamic exclusion criteria included mass widths of 5 ppm, a repeat count of 2 and a repeat duration of 6s. The MS^2 and MS^3 normalized collision energies were ramped over the range of 35 to 45%. Data acquisition and processing were carried out using Xcalibur software (version 1.3, Thermo Fisher Scientific).

The reaction phenotyping samples analysis was performed on LC–MS/MS AB SCIEX 5500 mass spectrometer system controlled by Analyst 1.4.2 software and equipped with Water Acquity UPLC. Chromatographic separations were performed on a UPLC column Acquity, BEH, C18, 1.7µm, 2.1×50mm; maintained at 40^{o}C temperature. The mobile phase consisted of solvent A (0.1% formic acid

in water) and solvent B (methanol) delivered at a flow rate of 0.4 ml/min with a linear gradient as follows: 10% to 30% B over 5min, 30% to 40% B from 5 to 6min, 40% to 50% B from 6 to 12min, 50% to 70% B from 12 to 28min, 70% to 95% B from 28 to 30min, decreased to 10% B from 30 to 32 min and maintained equilibrium up to 37 min.The MS was operated in the positive electrospray mode at a capillary temperature 550^{o}C; MS/MS analysis was performed using nitrogen as the collision gas and the collision energy was set from 40-60 eV.